Applied Thermal Engineering 220 (2023) 119701

Contents lists available at ScienceDirect

Applied Thermal Engineering

journal homepage: www.elsevier.com/locate/apthermeng

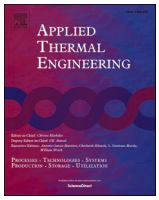

Research Paper

Repurposing a deep geothermal exploration well for borehole thermal energy storage: Implications from statistical modelling and sensitivity analysis

Christopher S. Brown *, Isa Kolo, Gioia Falcone, David Banks

James Watt School of Engineering University of Glasgow, Glasgow G12 8QQ, Scotland, UK

ARTICLE INFO

Keywords:
Newcastle Science Central Deep Geothermal Borehole (NSCDGB)
Borehole Thermal Energy Storage (BTES)
Borehole heat exchanger
MATLAB
Borehole thermal energy storage model
Repurposing
Numerical modelling
Statistical modelling

ABSTRACT

Borehole thermal energy storage (BTES) is an important technology to minimise greenhouse gas emissions by storing surplus heat from industrial processes, space cooling or even excess summertime renewable wind or solar energy. This paper investigates the efficiency of BTES via a single deep ex-geothermal exploration well in Newcastle, retrofitted using a coaxial deep borehole heat exchanger (DBHE) completion. Previously, few studies have investigated 1) the use of a single DBHE for thermal energy storage or 2) the retrofitting of an ex-geothermal exploration well; therefore, this study investigates deep BTES through numerical modelling on MATLAB by testing the impacts of 10 design parameters on operational performance of a DBHE using both global and local sensitivity analyses.

Under base-case conditions, a DBHE operating at a depth of 920 m could achieve a heat extraction rate in excess of c.54 kW recorded at the end of a 6 month (winter) heat production phase. When applying a 6 month (summer) thermal charge phase prior to extraction (recorded as 250 kW at the end of the charge period), the thermal yield recorded at the end of extraction was increased to a minimum of c.69 kW. In total, over an annual cycle, 1.23 GWh of heat was injected into the formation, and 0.46 GWh was extracted. Across all local sensitivity simulations, the average heat extraction rate was increased by 9.5–55.6 kW following a 6 month period of charge. The global sensitivity analysis demonstrated that thermal recovery was most influenced by parameters such as the undisturbed geothermal gradient, flow rate, inlet temperature during charge and inlet temperature during extraction. Most of these are operational parameters, indicating deep BTES systems can be optimised through careful engineering. The study concludes that single DBHEs have some capacity to store surplus heat. However, the additional heat yield during extraction is only a modest proportion of the heat reinjected to the formation during the charging phase (calculated as <20 % using the new storage efficiency metric proposed in this study). This approach is only likely to be viable where there is a large source of surplus heat with little alternative value, and where there is an existing deep borehole suitable for retrofitting. If these conditions do not exists, more conventional, shallower, multi-borehole arrays are likely to be more suitable for BTES.

1. Introduction

Renewable energy can be seasonal (i.e., solar, wind) or weather dependent (i.e., wind), leading to variations in energy supply; therefore, given the large demand for heat worldwide, alternative energy storage methods must be considered. Underground thermal energy storage (UTES) poses a significant opportunity to utilise the fluctuating thermal energy from the aforementioned renewable resources by transferring heat into the subsurface during low consumer demand months. UTES technology operates by storing heat in subsurface fluid and solid (aquifer thermal energy storage) (e.g., [27]) or in solid rocks only (via borehole thermal energy storage (BTES)) (e.g., [34]). This study focuses on deep BTES, where limited research evaluating the potential of deeper systems has been conducted.

Recent work has evaluated the potential of deep borehole heat exchangers (DBHE) for extraction only (e.g., [21,5,20,26,31,46,24,37,48,46]), whilst few have evaluated BTES for depths in excess of 1000 m. DBHEs operate by circulating fluid in the subsurface within a closed-circuit system. Typically, for coaxial DBHEs, a concentric tube is inserted within the borehole. Fluid is circulated

* Corresponding author.
E-mail address: christopher.brown@glasgow.ac.uk (C.S. Brown).

https://doi.org/10.1016/j.applthermaleng.2022.119701
Received 27 July 2022; Received in revised form 16 November 2022; Accepted 19 November 2022
Available online 24 November 2022

down the annular space, exchanging heat by conduction through the borehole wall to or from the surrounding rock. The fluid is then circulated to the surface through the central pipe, with advective heat transfer dominant. To be in line with other authors [52] for UK specific studies who have focused on well repurposing, we define the boundary between shallow and deep geothermal as 500 m, due to past UK Renewable Heat Incentives subsidies [44].

Extraction studies have shown that increasing the borehole depth disproportionately increases the achievable heat load due to the interplay of two factors: (i) increasing temperature due to the geothermal gradient, and (ii) a greater borehole length (and surface area) for heat exchange [15,61]. Therefore, the greater overall surface areas of deeper boreholes could also increase performance during energy storage. Modelling studies for BTES focus on shallow borehole heat exchanger (BHE) arrays and the impact of engineering design parameters, such as the number of BHEs in an array, array geometry, BHE spacing, BHE depth, material property variations and level of water saturation within the ground [55,60,63,49,51,59,9]. Some have gone further to investigate heat transfer in shallow geothermal piles, identifying the spiral configuration as an alternative heat exchanger with a high heat transfer efficiency [10,11]. Few focus on the idea of a single DBHE designed for BTES; this work therefore, aims to address this gap in literature. DBHEs may be more suited over shallow BHE arrays in areas where there is potential to repurpose a deep well without the initial capital expenditure required for drilling, or if there is a limited surface footprint for development.

Xie et al. [62] investigated the influence of 5 parameters on a single DBHE for BTES in a global sensitivity analysis. They concluded that the most important parameters, in order, were geothermal gradient, inlet temperature during charge, flow rate, rock thermal conductivity, and lastly, insulation thickness. Whilst this is an important study for furthering the knowledge of deep BTES systems, the limited range of parameters considered disregards important parameters such as piping material, grout material, inlet temperature during extraction, flow direction and depth of borehole. Furthermore, the study's focus was predominantly on the charge period, giving scope to investigate the performance during both the charge and extraction periods. As a result, this paper aims to meet the gap in literature by considering a wider variety of parameters and explore single deep BTES systems in further detail.

A further subset of this study was to investigate the evaluation metric for storage efficiency. This is commonly defined in shallow BTES arrays as the ratio of energy extracted to stored (e.g., [19,34,59]). Few, if any, have investigated this metric for storage efficiency for deep systems focusing on single well storage. Xie et al. [62] evaluated the storage efficiency for the charge period of a single DBHE for BTES, without accounting for the extraction period. Therefore, this paper adds further value and novelty by investigating the most suitable metric for evaluating storage efficiency in deep BTES systems by comparing previously used metrics and a new metric (further detailed in section 2.4).

The Newcastle Science Central Deep Geothermal Borehole (NSCDGB) was selected as a case study in this paper due to: 1) high heat flows which are observed in the area and are associated to geothermal resources of the North Pennine Batholith, leading to high bottom-hole temperatures [64,33,18], 2) the well has already been drilled and therefore, would require limited cost to convert to a coaxial DBHE, which could unlock a technology that has previously had economic limitations [57] and 3) it is proximal to multiple buildings, such as the Urban Science Building (e.g., [65]), which have a demand for heat. Furthermore, there is also potential to feed the thermal energy into a heat network or smart energy system (e.g., [39]), such that the DBHE can act as a balancing component. This work was undertaken as part of the EPSRC project "NetZero GeoRDIE – Net Zero Geothermal Research for District Infrastructure Engineering (Grant No EP/T022825/1)" [29]. The project plans to repurpose the borehole as a pilot DBHE within the UK and it is envisioned that the model results from this study will facilitate DBHE testing.

The NSCDGB is located in Newcastle in the northwest of England (Fig. 1) to a total depth of 1821 m [64]. It was drilled as a vertical exploratory geothermal well between 2011 and 2014, targeting the Mississippian Fell Sandstone Formation, which proved to have low hydraulic conductivity and would consequently not be suitable for development via conventional "wet sedimentary reservoir" methods [64]. The borehole intersects a thick succession of Carboniferous strata and was cased to depths of just over 900 m. A narrow diameter liner (4.5 in./~11.4 cm) was inserted below 922 m, which makes circulation of a heat transfer fluid below that depth hydraulically unattractive; although it is worth noting repurposing options remain available at higher costs at greater depths. Therefore, to minimise further cost during conversion, the initial base case scenario for the analysis was set as 920 m. To test the potential of the NSCDGB as a DBHE, variations in borehole depth, inner pipe thermal conductivity, outer pipe thermal conductivity, grout thermal conductivity, rock thermal conductivity, flow rate, thermal gradient, inlet temperature during extraction, inlet temperature during charge and flow direction were all modelled. While the initial base case parameters were specific to data obtained from the NSCDGB, the parameter range tested is more generic to test the potential for deep BTES systems worldwide. In real operating conditions it is likely that a heat load will be imposed on the system, in this case we use constant inlet temperatures, such that the likely average heat rate or load of the system can be calculated for varying parameters. This will then be used to inform future surface models aiming to integrate the surface operation with the subsurface.

The model used in this study was designed on MATLAB by Brown et al. [15]; it uses a series of 1D nodes to replicate the borehole heat exchanger components and is integrated in a 3D nodal domain for the subsurface rock. This approach saves computational time and the scripting on MATLAB allows repeat analysis to evaluate the impact of a variety of parameters for energy storage. Simulations were run for an annual time period, with 6 months charge and 6 months extraction. These time periods are considered typical for 'cooling' and 'heating' periods in the UK (e.g., [13]). The model was compared to OpenGeoSys

Fig. 1. Map of the UK highlighting wellbore location in Newcastle.

software to test the validity of the solution as a benchmarking assessment, whilst the heat flux in the model between grout and solid rock was also compared to the heat load leaving the model for additional validation. The model has been tested further against analytical solutions and case studies (see [14,15]). Both local and global sensitivity analyses were undertaken to establish the most influential parameters on energy storage and heat transfer.

In the UK, there is a significant amount of oil and gas wells that are plugged, abandoned or entering the latter stages of production which could therefore be repurposed for deep geothermal exploitation [52,53]. Whilst this study focuses on the repurposing of an old geothermal exploration well, it has national and international connotations on the repurposing of existing deep hydrocarbon wells (or unproductive deep exploration wells for hydrocarbons / conventional geothermal resources), where this form of technology has had limited development for energy storage. A broad range of parameters were tested, giving estimates for heat rates without charge, heat rates with charge, total energy stored/extracted and the efficiency of BTES systems.

The work in this study will have direct local relevance as it will indicate whether DBHEs could contribute to heating and cooling of adjacent buildings in the Newcastle area and, if so, the most efficient mode of operation. It will also have wider implications for thermal energy storage in terms of optimisation of the design for retrofitting heat exchange infrastructure to repurposed wells. Within literature there is also a lack of investigation into deep BTES systems via DBHEs; moreover, typically metrics utilised for evaluating thermal storage appear to be poorly suited to deep systems as they are commonly used for shallow BTES. A new metric is proposed in this study which can be universally applied to both deep and shallow studies. Therefore, to summarise, this study aims to identify the parameters to which efficient operation of BTES via DBHEs is most sensitive, whilst also considering alternative metrics of evaluating storage efficiency. This paper has further novelty, by investigating the performance of a repurposed deep geothermal exploration well as a DBHE. This may provide a method of de-risking geothermal developments by providing an alternative solution for energy exploitation if the system is not suitable for open-loop development.

2. Methods

2.1. Governing equations

The model assumes heat transfer in the subsurface is dominated by conductive heat flux. To test the impact of varying model parameters, the rock was assumed to be homogenous. The presence of groundwater was observed in the shallow portion of the NSCDGB. However, the influence of this was not modelled due to 1) the shallowest water encountered was associated to a perched aquifer 20 m below ground level, 2) further water was associated to complex fractures, which were not tested for permeability and data is unavailable, 3) water bearing rocks at increased depths exhibit extremely poor hydraulic conductivity ($\sim 5.4 \times 10^{-10}$ m/s) [64], 4) it has been suggested the impact of groundwater on DBHEs is minimal [20], and 5) the results of the study can be extended to more universal applications. Therefore, conductive heat flux can be modelled as (e.g., [43,33]):

$$\frac{\partial T}{\partial t} = \alpha \nabla^2 T \quad (1)$$

where T is the temperature, t is time and α is the thermal diffusivity of the rock (see Table 1 for the NSCDGB case study).

Heat transfer in the borehole was modelled using the 'Dual-Continuum' approach [32,20] and, as highlighted in Fig. 2, uses a series of nodes in a 1D line designed to simulate heat flow in the borehole between the fluid, pipes, grout and surrounding rocks (e.g., [2,3,4,1,22,23,41,42]). This allows a reduced computational time in comparison to a fully discretised solution, with heat flux in the vertical direction acting across the cross sectional area (left hand side of eq. 2–5) and heat flux across the horizontal using thermal resistance (right hand side of eq. 2–5) (Fig. 3). The model was implemented on MATLAB by Brown et al. [15] using the finite-difference method. In this study, the model is utilised to understand BTES of deep systems and a simulation time for a model run of a year is typically less than 30 min.

Table 1
Nomenclature and thermo-physical parameters of the model. Model parameters are either taken from literature, assumed unpublished values (assembled by Westaway [58] and Banks [8], calculated values or given as the most likely value. Literature sources were: Younger et al. [64], Kimbell et al. [66], Westaway and Younger [56], Brown et al [15], Gebski et al. [28], Bott et al. [12], England et al. [25] and Lesniak et al. [36]. Note the inner pipe is the coaxial pipe and the outer pipe is the casing. The real nature of the casing situation is notably more complex than that modelled.

Parameter	Value	Units	Symbol
Borehole Depth [64]	920	m	–
Borehole Diameter [64]	0.216	m	$2\pi r_{pi}$
Outer Diameter of Inner Pipe	0.1005	m	$2\pi r_{po}$
Thickness of Inner Pipe	0.00688	m	–
Thickness of Outer Pipe	0.0081	m	–
Thickness of Grout	0.01905	m	–
Thermal Conductivity of Polyethylene Inner Pipe	0.45	W/(m.K)	–
Thermal Conductivity of Steel Outer Pipe	52.7	W/(m.K)	–
Density of Rock [66]	2500	kg/m^3	ρ_s
Thermal Conductivity of Rock [12,25,28,64]	2.925	W/(m.K)	λ_s
Specific Heat Capacity of Rock [36,56]	1300	J/kgK	C_s
Density of Grout	995	kg/m^3	ρ_g
Thermal Conductivity of Grout	1.05	W/(m.K)	λ_g
Specific Heat Capacity of Grout	1200	J/kgK	C_g
Density of Fluid [15]	998	kg/m^3	ρ_f
Thermal Conductivity of Fluid	0.59	W/(m.K)	λ_f
Specific Heat Capacity of Fluid	4179	J/kgK	C_f
Fluid Injection Temperature (charge)	95	°C	T
Fluid Injection Temperature (extraction)	10	°C	T
Surface Temperature [28]	9	°C	–
Geothermal Gradient [28,64]	33.4	°C/km	–
Volumetric Flow Rate	0.00833	m^3/s	h

Heat flux between the central co-axial pipe, annulus and grout can be calculated as:

$$\rho_f C_f \frac{\partial T_{po}}{\partial t} A_{po} - \lambda_f \frac{\partial^2 T_{po}}{\partial z^2} A_{po} - \rho_f C_f u_{po} \frac{\partial T_{po}}{\partial z} A_{po} = b_{poi}\left(T_{pi} - T_{po}\right) 2\pi r_{po} \quad (2)$$

$$\rho_f C_f \frac{\partial T_{pi}}{\partial t} A_{pi} - \lambda_f \frac{\partial^2 T_{pi}}{\partial z^2} A_{pi} + \rho_f C_f u_{pi} \frac{\partial T_{pi}}{\partial z} A_{pi} = b_{poi}\left(T_{po} - T_{pi}\right) 2\pi r_{po} + b_{pig}\left(T_g - T_{pi}\right) 2\pi r_{pi} \quad (3)$$

$$\rho_g C_g \frac{\partial T_g}{\partial t} A_g - \lambda_g \frac{\partial^2 T_g}{\partial z^2} A_g = b_{pig}\left(T_{pi} - T_g\right) 2\pi r_{pi} + b_{sg}\left(T_s - T_g\right) 2\pi r_g \quad (4)$$

$$\rho_s C_s \frac{\partial T_s}{\partial t} A_s - \lambda_s \frac{\partial^2 T_s}{\partial z^2} A_s = b_{sg}\left(T_g - T_s\right) 2\pi r_g \quad (5)$$

where ρ is the density, C is the specific heat capacity, A is for area, r is the radius, λ is the thermal conductivity, u is the velocity, T_{pi} is the temperature of the fluid in the annular space and b_{pig} is the reciprocal of thermal resistance (i.e., conductance) between the pipe and grout. The value for the reciprocal of thermal resistance can be calculated as a constant value from the fluid flow (which accounts for turbulence, which in this study is always in excess of a Reynolds number of ~ 7000), material conductivity and thickness. Subscript f is for fluid in the central pipe or annulus, po is for the central pipe out, pi is for the annular space,

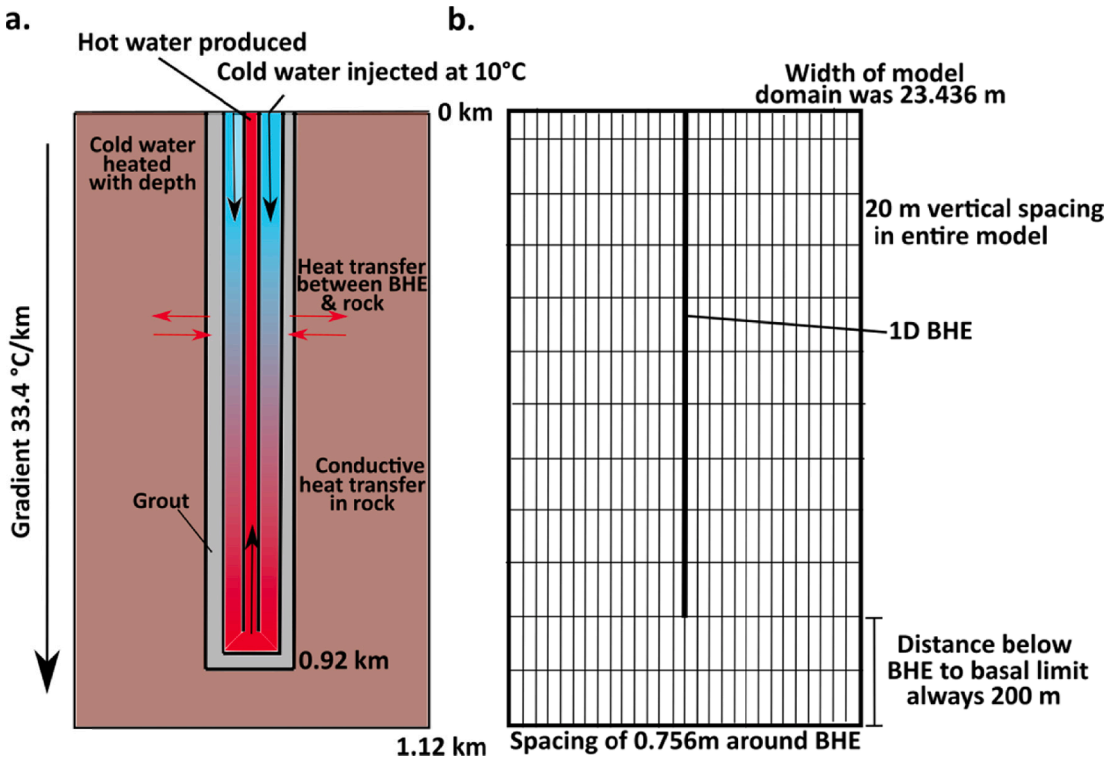

Fig. 2. (a) Schematic of the coaxial DBHE (with normal flow direction – CXA heat exchanger), and (b) the discretised nodal domain (modified after [15]).

g is for grout and s is for solid rock. The respective parameters and symbols can also be found in Table 1. Further information on model design is available in Brown et al. [15]. A simple flow chart highlighting the model processes can be found in Fig. 4.

2.2. Initial, boundary and operational conditions

The model domain was discretised on a Cartesian grid which extends to a depth of 1120 m using uniform 20 m vertical spacing with the DBHE reaching a depth of 920 m (Fig. 2). The lateral domain was tested to ensure that no boundary interactions would occur during the annual simulation. As highlighted in Fig. 5a, it was observed at the end of extraction and charge periods minor boundary interference occurs when the domain boundary is $\leq$ 19 m away from the DBHE. Therefore, boundaries were extended to be larger than this for all simulations with the radial distance from the DBHE to model boundaries set at 23.436 m. The lateral nodal spacing around the DBHE was set at 0.756 m.

At the surface level, it was assumed there was no heat flux or thermal interactions through the boundary, whilst the model base and sides were assumed to be at constant temperature as predicated by the geothermal gradient. Under initial conditions, the geothermal gradient was assumed to be linear and the BHE components were in equilibrium with the surrounding rock $\left(T_s = T_g = T_p = T_f\right)$. The surface temperature of the model was also assumed to equal the average ground surface temperature throughout the year. For the base case scenario, inlet temperature was fixed at 10 °C during extraction and 95 °C during charge. Although DBHEs usually use a predefined heat load from the heat pump, in this study, we are interested in identifying achievable heat loads/rates based on parameterisation, which will act as a guide for future development of the DBHE and nearby buildings. Therefore, the average thermal power was calculated during charge and extraction giving an estimation of the likely heat load that could be applied.

The operation of the DBHE utilised the inlet in the coaxial annular space (CXA) for the base case scenario for both charge and extraction (Fig. 2a). A total of four different configurations of flow direction for DBHE operation were considered: 1) inlet through the annular space for charge and extraction (CXA), 2) reverse flow direction of the DBHE (CXC) (i.e., inlet through the central pipe for both charge and extraction – Fig. 3), 3) reverse flow for charge (CXC) and normal flow for extraction (CXA), 4) normal flow for charge (CXA) and reverse flow for extraction (CXC).

2.3. Model benchmarking

The model was tested against OpenGeoSys (OGS) software for discrepancies in results. In OGS, the model domain was created and meshed using Gmsh via a pre-processing tool available as an executable file [50]. A domain size of 100 m by 100 m by 1418.5 m was applied (x,y,z). The model was set up identically to MATLAB with the DBHE centralised within the domain and constant temperature boundary conditions imposed on all lateral boundaries. At surface level and the base of the model there was no heat flux or thermal interactions through the boundary. The model was implemented using the base case parameters listed in Table 1 to test both charge and extraction (0 < t less than 182.5 days, T_{in}=95 °C and 182.5 < t less than 365 days, T_{in}=10 °C). As highlighted in Fig. 5b, the models have a near identical match. After the first few days of the simulation the difference in outlet flow temperatures for the duration of the simulations is less than 0.3 °C. This corresponds to a maximum discrepancy in outlet temperatures of less than 0.3 % between solutions.

Another form of validation was considered by comparing the balance and accuracy of the model over a time step (similar to the method of [20]). The heat flux between the grout and solid rock can be integrated over the length of the DBHE and compared to the heat flux leaving the model (Eq. 6). The values indicate the model is capable of producing accurate results with a discrepancy of 1.5 %. This equates to a difference of 2 kW.

2.4. Evaluation of performance

The thermal performance of the DBHE was determined by considering the heat rate or thermal power (P) during both charge and

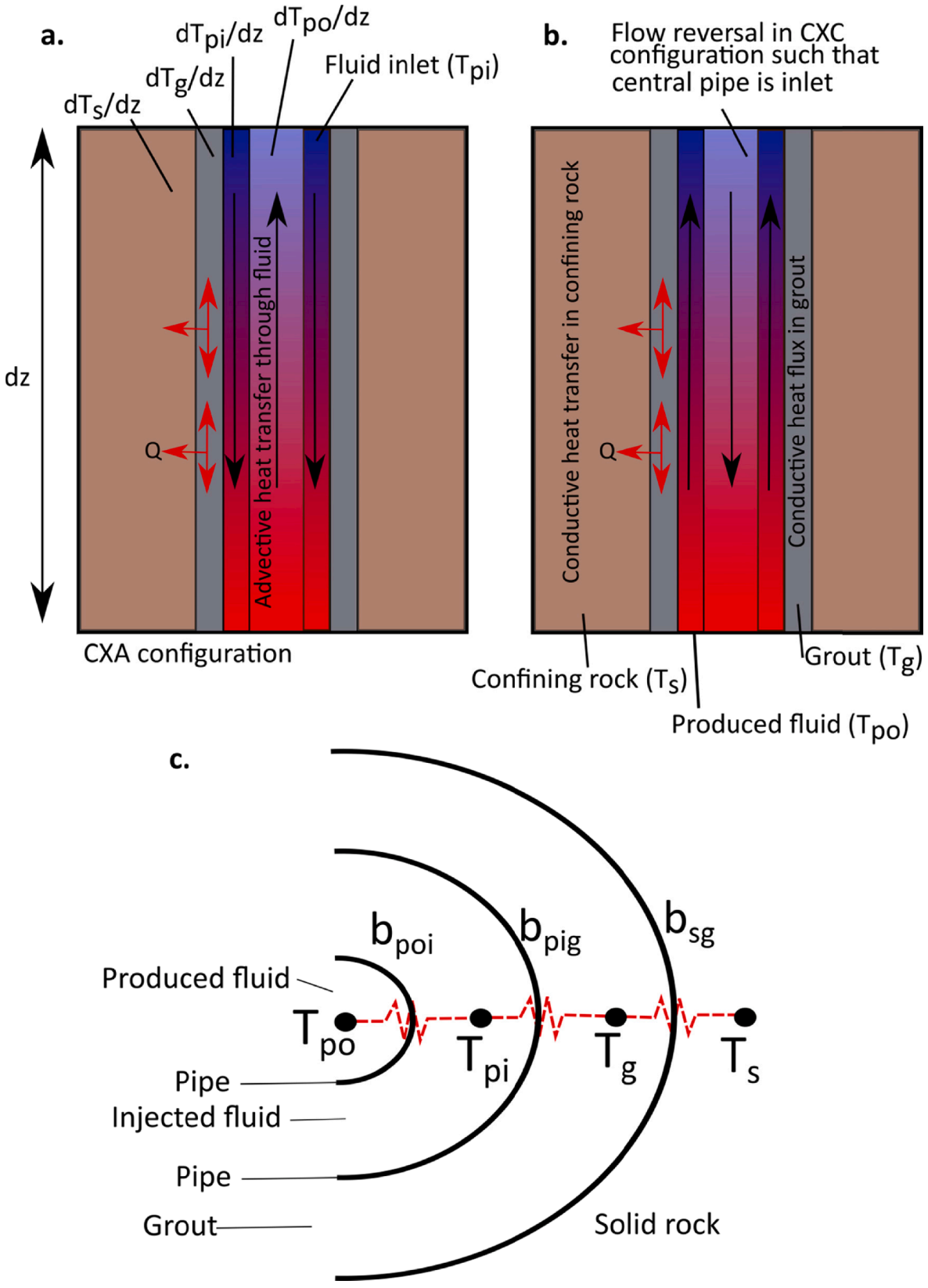

Fig. 3. (a) Schematic of the heat flux in a normal flow direction (CXA) coaxial DBHE, (b) schematic of the heat flux in a reverse flow direction (CXC) coaxial DBHE and (c) reciprocals of thermal resistance for the CXA setting (modified after [15]).

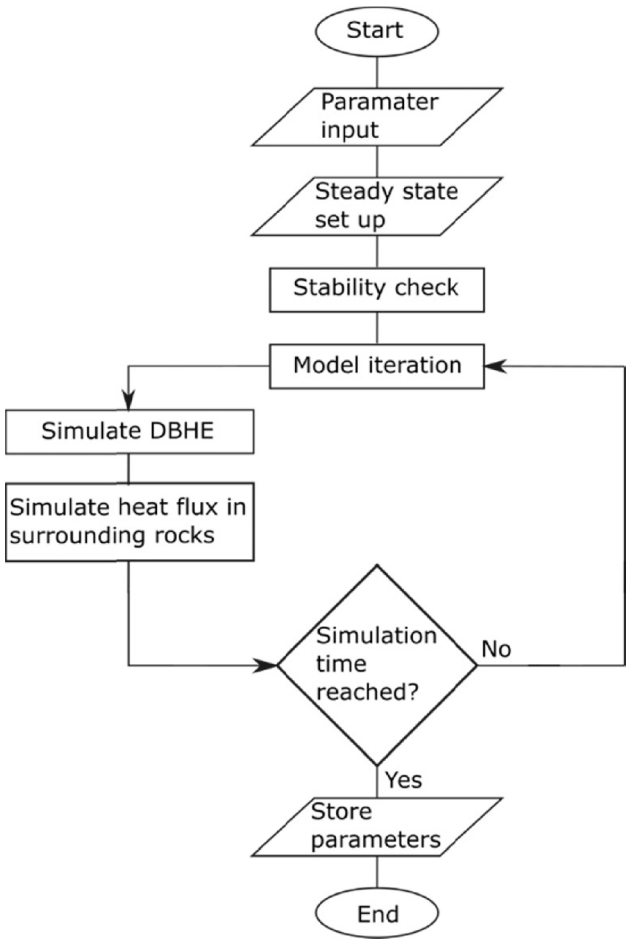

Fig. 4. Simple flow chart highlighting model processes.

extraction (e.g., [21,40]):

$$P = \rho_f c_f Q(T_{out} - T_{in}) \quad 6$$

where Q is the volumetric flow rate. During extraction, the heat rate would typically be positive indicating heat is transferred from the subsurface to the fluid in the DBHE, whilst during charge it is likely to be negative, indicating transfer of heat between the fluid in the DBHE, through the casing/cementitious grout and into the surrounding solid rock in the subsurface.

Storage efficiency can help to evaluate performance and is commonly determined in literature for shallow arrays ($SE_{shallow}$) (and some deeper arrays - [54,55]) by calculating the total energy extracted divided by the total energy injected (e.g., [19,34,59]). This is analogous to taking the average heat transfer for both the charge and extraction phases of the simulation. Assuming the mass flow rate and volumetric heat capacity of the fluid are equal during charge and extraction, storage efficiency ($SE_{shallow}$) can be simplified to:

$$SE_{shallow} = \frac{\text{Total } P_{extraction}}{\text{Total } P_{storage}} = \frac{\overline{\Delta T_{extraction}}}{\Delta T_{charge}} = \left|\frac{\overline{T_{out} - T_{in}}}{T_{out} - T_{in}}\right| \quad 7$$

This method was used for evaluating results (in section 3.2 and 3.3) and then further consideration was given to new and alternative methods (Eq. (8) and (9)) of evaluating storage efficiency (section 3.4). New and alternative methods were tested as Eq. (7) does not necessarily represent the true nature of storage in a system (i.e., how much of the energy injected is truly recovered), but more so the system efficiency.

Xie et al. [62] defined an alternative metric for storage efficiency for the charge period of deep systems. The storage efficiency (SE_{charge}) can

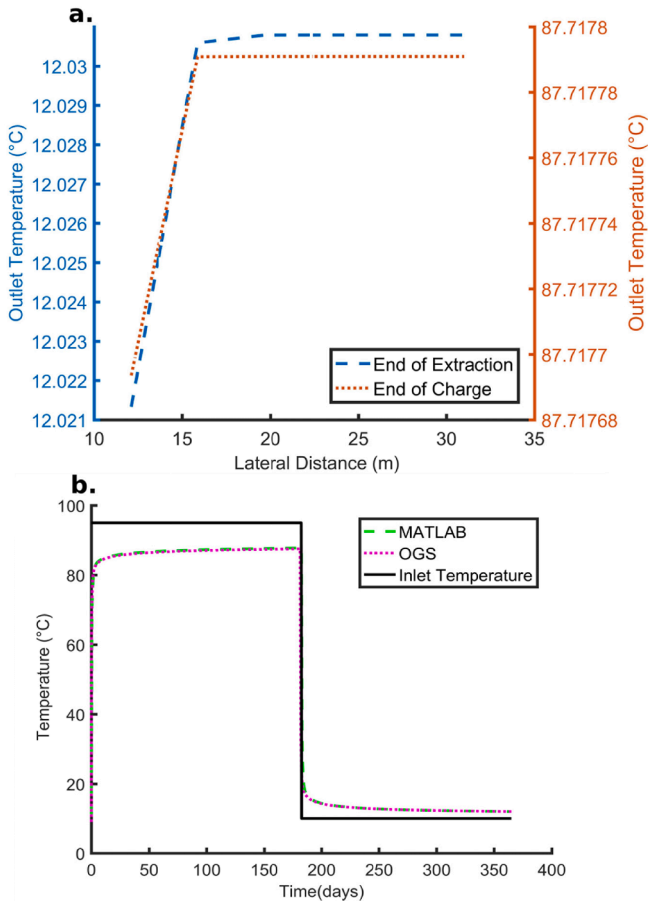

Fig. 5. (a) Plot comparing the impact of setting different radial boundary domain limits from the central DBHE (lateral distance) on the final outlet temperature at the end of charge and extraction. (b) Comparison of MATLAB with OGS (OpenGeoSys) for outlet temperatures for the base case, with the inlet temperature for both highlighted in black.

be defined as:

$$SE_{charge} = \frac{Q(h_{in} - h_{out})}{Qh_{in}} \quad 8$$

where h represents the fluid enthalpy and the subscripts represent the inlet and outlet. A new method of storage evaluation was also considered here, which evaluates the increase in energy extracted during the production period in proportion to heat injected. This is defined as the absolute difference between average heat extraction rates (P) with and without charge (SE_{new}):

$$SE_{new} = \frac{\text{Total } \Delta P_{extraction}}{\text{Total } P_{charge}} = \left|\frac{\left(\rho_f c_f Q(T_{out} - T_{in})\right)_{pc} - \left(\rho_f c_f Q(T_{out} - T_{in})\right)_{nc}}{\left(\rho_f c_f Q(T_{in} - T_{out})\right)_{charge}}\right| \quad 9$$

where the subscript pc is for the thermal power post charge and nc is for the thermal power with no charge. Whilst we are testing this metric for DBHEs it could be used to highlight the recovered energy from a shallower system.

When analysing the data for the global simulations, Spearman's Rank Correlation (SRC) was used to obtain the influence of a parameter on the storage efficiency (shallow method) and heat rate. Spearman's Rank can be calculated as:

$$SRC = 1 - \frac{6\sum_{j=1}^{n}\left[R(X_j) - R(Y_j)\right]^2}{n(n^2 - 1)} \quad 10$$

where $R(X_j)$ is the rank of different parameters, $R(Y_j)$ is the rank of the simulated result (i.e., storage efficiency (shallow) and heat rate) and n is the sample size (300 - limited due to computational demands). Pearson's Correlation Coefficient (PCC) was also used to determine the relationships between two variables (X and Y) and can be solved as:

$$PCC = \frac{n\sum X_i Y_i - \sum X_i \sum Y_i}{\sqrt{n\sum X_i^2 - (\sum X_i)^2}\sqrt{n\sum Y_i^2 - (\sum Y_i)^2}} \quad 11$$

2.5. Modelling parameters for local and global sensitivity analysis

When considering both local and global sensitivities, models were parameterised between potential maximum and minimum limits of geological, operational and engineering parameters based on known data or from literature. These are summarised in Table 2. During local simulations, each parameter was tested individually, whilst for the global simulations all parameters were randomly assigned using a uniform distribution of probability density. Additionally, during the local sensitivity analysis, the bottom two parameters listed in Table 2 (inlet temperature during charge and flow direction) were only applied to energy storage solutions. Furthermore, when increasing the borehole depth the basal limit of the model was always 200 m away from the base of the DBHE. The local parameters listed in Table 1 were adopted for geological and engineering properties from Bott et al. [12], England et al. [25], Kimbell et al. [66], Lesniak et al. [36] and Westaway and Younger [56]. Thermal conductivity estimates calculated during the initial drilling campaign within the borehole are limited to depths in excess of 500 m, therefore, homogenous rock properties were used. Variations in thermal conductivity were accounted for in the borehole by applying a range of values between 1.5 and 4.5 W/(m.K); the former associated to lower thermal conductivity shallower sediments and the latter to the maximum values within the Stainmore Formation (see [64]). The charge inlet temperatures correspond to temperatures used in BTES schemes around the world (e.g., see the heat store project - [30]). Typically, charge temperature should be higher than the average undisturbed ground temperature to ensure heat is stored, rather than extracted.

3. Results

3.1. Temporal variations during charge and extraction

During the initial period of charge, the DBHE showed a rapid cooling of the fluid as it progressed down the annulus (Fig. 6a). As the outlet temperature was near equal to surface temperature under initial conditions, there was an overall increase of the outlet temperature of the fluid (Fig. 5b). After ~ 1 month, the outlet temperature reached a quasi-steady state, highlighting that a steady-state heat flow field in the surrounding rocks in proximity to the borehole was established (Fig. 5b, 6a & 6c). The surrounding rock showed minimal thermal propagation around the DBHE (within 10 m) and a sharp concaving downwards of the thermal front (Fig. 7a & 7b). At the end of the 6 months charge period, the outlet temperature was 87.77 °C, achieving a thermal power of −250.3 kW and a total of 1.23 GWh of heat stored. This highlights heat from the DBHE fluid was being transferred to the surrounding rocks and warming the subsurface.

In contrast, the period of extraction following charge showed a rapid cooling of the DBHE and exponential decline of the outlet temperature (Fig. 5b and 6b). The surrounding rock also showed thermal propagation was confined to within ~ 15 m of the DBHE with sharp concaving upwards, shallowing near the surface (Fig. 6d, 7c & 7d). It was also evident that thermal perturbations were still propagating away from the DBHE following the period of extraction, highlighting not all the energy stored had been extracted. At the end of the 12 month simulation, the final outlet temperature was 12.01 °C, achieving a thermal power of 69.5 kW and a total of 0.46 GWh of heat extracted. This equates to a storage efficiency of ~ 0.37.

Table 2
Parameters used for local and global sensitivity studies. *Flow direction was based on 4 cases: 1) CXC charge, CXC extraction 2) CXC charge, CXA extraction 3) CXA charge, CXA extraction 4) CXA charge, CXC extraction. For Flow direction these were not randomised and instead allocated 75 runs for each.

Parameter	Units	Minimum	Maximum
Borehole Depth	m	100	2500
Inner Pipe Thermal Conductivity	W/(m.K)	5	50
Outer Pipe Thermal Conductivity	W/(m.K)	5	50
Grout Thermal Conductivity	W/(m.K)	0.5	5
Rock Thermal Conductivity	W/(m.K)	1.5	4.5
Flow Rate	L/s	1	8
Geothermal Gradient	°C/km	10	40
Inlet Temperature (Charge)	°C	30	90
Inlet Temperature (Extraction)	°C	5	25
Flow Direction*	–	CXC	CXA

3.2. Local sensitivity

3.2.1. Extraction only

As highlighted in Fig. 8 (solid blue line), during a period of extraction only, it was observed that the average heat rate is relatively low (less than 358 kW and typically under 80 kW for depths of 920 m – equivalent of 1.55 and 0.35 GWh of heat extracted, respectively) in comparison to other conventional deep geothermal applications, where the thermal power can be multiple orders of magnitude higher (>3 MW) (e.g., [35,16,17]). Borehole depth appears to be the most influential parameter with an exponential increase in heat rate with increasing depth due to the combined effects of increasing temperature and increased heat exchange length (Fig. 8b). Therefore, greater depths will lead to more extractable energy. Present plans are to temporarily repurpose the well using a retrievable tube for research purposes to a depth of c. 920 m due to casing limitations. However, the results indicate that if cost effective, it may be better to increase the depth of DBHEs when repurposing.

Flow rate, geothermal gradient, rock thermal conductivity and inlet temperature also showed strong influence on heat rate with variations of up to 82 kW between minimum and maximum parameters modelled (0.35 GWh of heat extracted) (Fig. 8c, e, f and g). The former three showed positive correlations with increasing parameter values resulting in higher heat rates and total heat extracted. Whilst higher flow rates correlated to higher heat rates, it is worth noting that these will be unsustainable in the long-term due to higher thermal drawdown and a reduced coefficient of system performance (e.g., [15]). The latter parameter (inlet temperature) corresponded to decreasing heat rates with increasing inlet temperatures. When the inlet temperature was 25 °C, it resulted in a negative thermal power highlighting more energy was being stored in the subsurface than was extracted. This was due to the fact that the inlet temperature was greater than the average formation temperature of 24.36 °C.

Other parameters do appear to have a more limited influence on results with outer pipe, inner pipe and grout thermal conductivity affecting the average heat rate to change by less than 15 kW over the operational period for the range of parameters modelled (Fig. 8a, d and h).

3.2.2. Energy storage

When a 6 month period of extraction followed a 6 month period of charge the average heat rate during the extraction period was significantly increased relative to the scenario described above (3.1). The average extraction heat rate increased by 9.5–55.6 kW across all parameters (red dashed line in Fig. 8). Most parameters showed a near uniform increase in heat rate; however, flow rate showed a limited increase when it was less than 2 l/s. This was due to more thermal interference between both the annular space and central pipe with

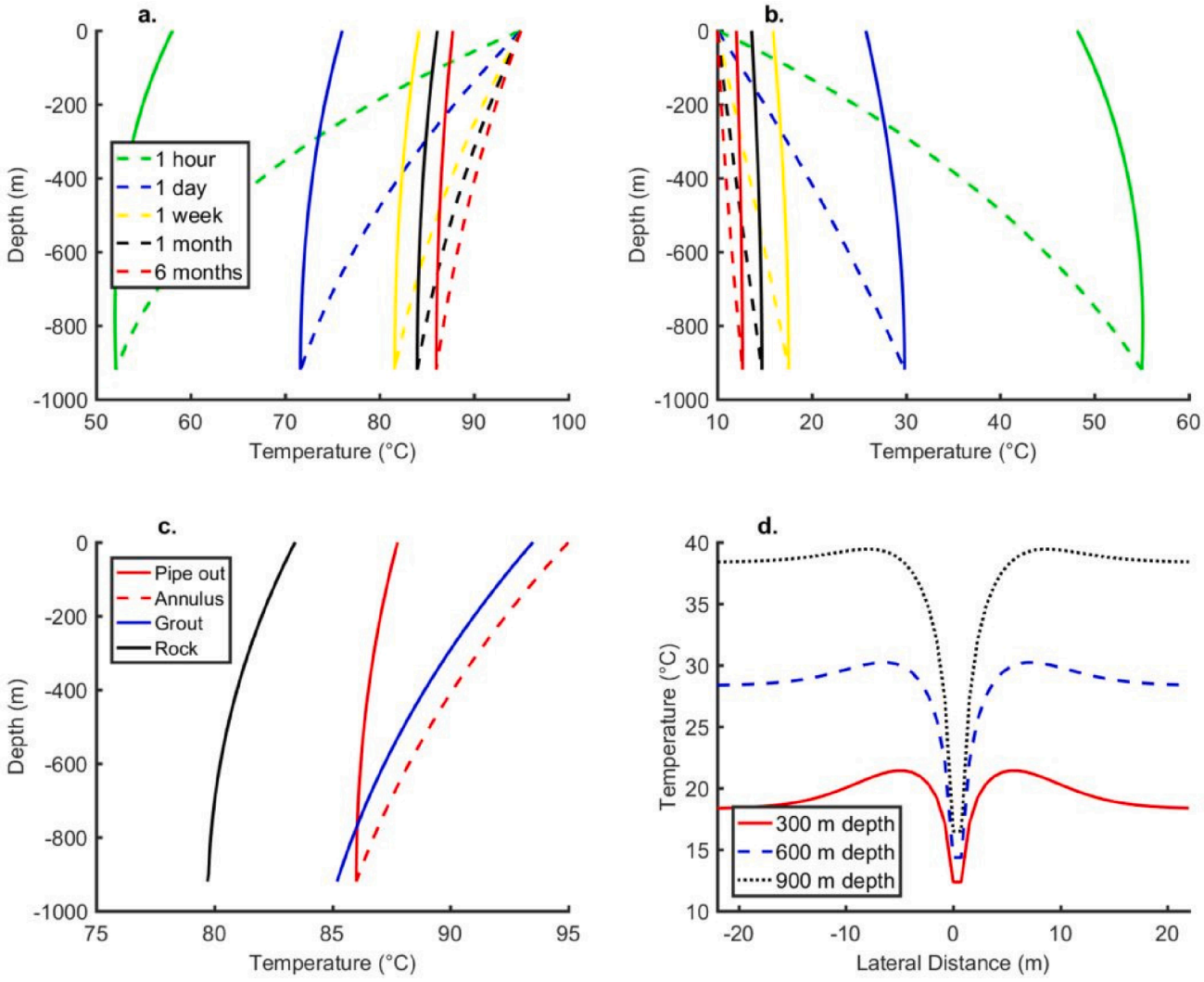

Fig. 6. Fluid temperature changes in the annulus (dashed line) and central pipe (solid line) during charge (a) and subsequent extraction (b). Note legend in (a) shows time scales for both plots. (c) Temperature of pipe out, annulus, grout and rock at the nodal points for the 1D DBHE with depth at the end of the charge period. (d) Thermal profile through the rock at the end of the simulation.

reduced velocities within the DBHE. Similarly, the average heat rate increased with increasing grout and rock thermal conductivity. This was due to more heat transfer around the DBHE during charge and extraction.

The heat transfer rate during the charge period was more significant than during extraction with the average heat rate (green dotted line in Fig. 8) ranging between −41.2 and −396.8 kW (0.18 and 1.71 GWh of heat injected, respectively). The greater heat transfer rates during charge in comparison to extraction were due to higher temperature differences between the inlet fluid temperature and average rock temperature. During charge, more heat transfer from the circulating fluid to surrounding formation were observed with increasing borehole depth, outer pipe thermal conductivity, rock thermal conductivity, flow rate, grout thermal conductivity and charge inlet temperature (Fig. 8b, d, e, f, h and 8a). Although an increase in borehole depth resulted in an exponential decline in heat rate up to 2000 m depth, it then appeared to increase further with depth. This was because the maximum heat transfer area was reached at c. 2000 m. Beyond this depth, the formation becomes hotter than the heat transfer fluid and heat is gained to the borehole in its deepest portions, rather than rejected. Increases in inner pipe thermal conductivity and geothermal gradient showed a reduction in heat transfer between the fluid in the borehole and subsurface rocks. This was because the former allows greater heat transfer between the central pipe and annular space leading to less heat transfer out of the DBHE, whilst the latter results in reduced temperature differences with depth in comparison to the inlet fluid temperature. Therefore, less heat can be transferred.

Flow Direction had minimal impact on performance; however, when the inlet was through the central pipe (CXC – see Fig. 3) during charge more heat was transferred into the subsurface. This was reflected by a decrease in outlet temperature by 0.4 °C at the end of the storage period in comparison to the normal flow direction coaxial annular heat exchanger (CXA) (Fig. 9b). This indicates more energy was stored during charge. Similarly, when having the inlet through the annular space (CXA) during extraction outlet temperatures at the end of the simulation were increased by 0.015–0.2 °C. An interesting phenomenon was also observed when flow direction was reversed and is highlighted in Fig. 9b as a spike at the end of charge. This occurred due to the previously hot fluid in the inlet during charge being removed immediately upon flow direction reversal. The outlet temperatures then followed the typical exponential decline observed in DBHEs during operation.

Interestingly, when considering the storage efficiency (Eq. (7)), it appears as though it is better to store energy using normal conventional flow (i.e., inlet through the annular space and outlet in the central pipe) (Fig. 10). This is the opposite of what the individual analysis of the charge and extraction period imply, with injection appearing best with

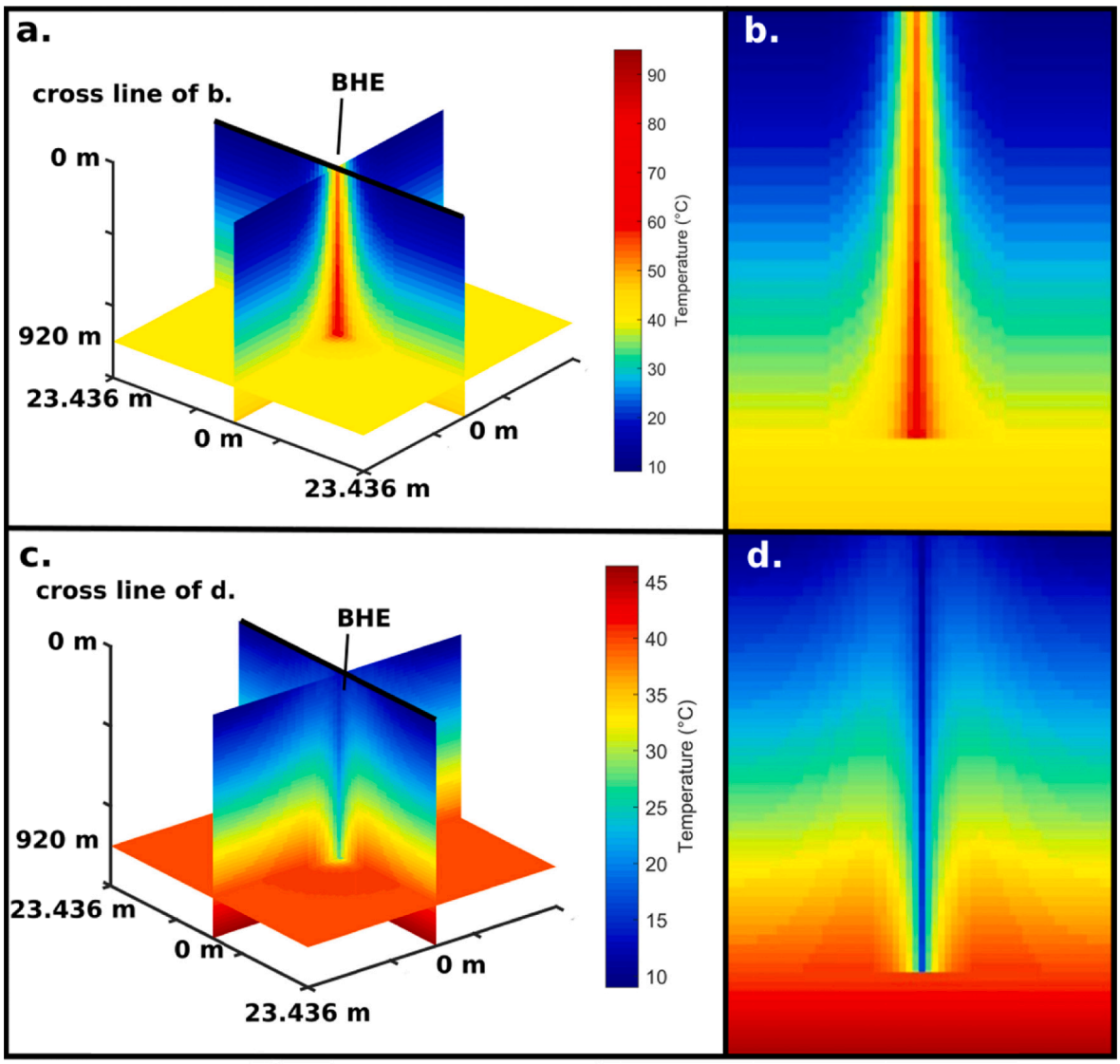

Fig. 7. (a) 3D and (b) 2D thermal profiles of the subsurface around the deep borehole heat exchanger (DBHE) after 6 months of charge. (c) 3D and (d) 2D thermal profiles of the subsurface around the DBHE after 6 months of extraction (following 6 months charge). Note for the 3D plots the borehole is located at point 0,0 for x,y.

reverse flow direction and extraction with normal. The reason for this result is strongly influenced by the evaluation method for storage efficiency. The poor storage during charge and better performance during extraction lead to a better apparent efficiency or recovery. This is tested further in section 3.4.

When considering the storage efficiency (Eq. (7)) for all other parameters, the thermal conductivity of the DBHE materials and surrounding rock had minimal impact, with a difference of less than 0.05 for the minimum and maximum respective parameters (Fig. 10). The negative decrease in storage efficiency observed for rock thermal conductivity was due to more heat being stored and proportionally less being recovered. This increase of storage and lateral thermal propagation away from the DBHE has been observed in case studies leading to negative impacts on the system [6,7]. The most influential parameters on storage efficiency were flow rate, extraction inlet temperature, charge inlet temperature, borehole depth and geothermal gradient (Fig. 10). Increasing the flow rate led to reduced thermal interaction between the central pipe and annular space, whilst altering the extraction and charge inlet temperatures increased the capacity and supply of energy, respectively. Borehole depth approached a storage efficiency in excess of 1 with increasing depth (Fig. 10b) which indicated all heat transferred into the system was extracted. Similarly, an increasing geothermal gradient appears to have a strong positive correlation to storage efficiency.

3.3. Global sensitivity

The previous section focused on more qualitative descriptions and data aggregation to understand parameters' influence; however, this section utilises quantitative methods by using Spearman's and Pearson's correlation coefficients. The former can be used for nonlinear monotonic relationships (e.g., [60]) and the latter for linear relationships [45]. The Monte Carlo method was used to generate the random parameter values in Table 2 on MATLAB and the frequency distribution is shown in Fig. 11. The distribution was uniform and all parameters were covered throughout the simulations. In this section it is also worth noting that for some cases, no heat was stored or extracted in the charge and extraction phases respectively, therefore when calculating the storage efficiency (Eq. (7)) for these cases, the value was set as zero.

3.3.1. Parameter rankings

The relationship between Spearman's and Pearson's correlation coefficients is shown in Fig. 12a with a good agreement between both methods. Results indicated one outlier for the storage efficiency of the

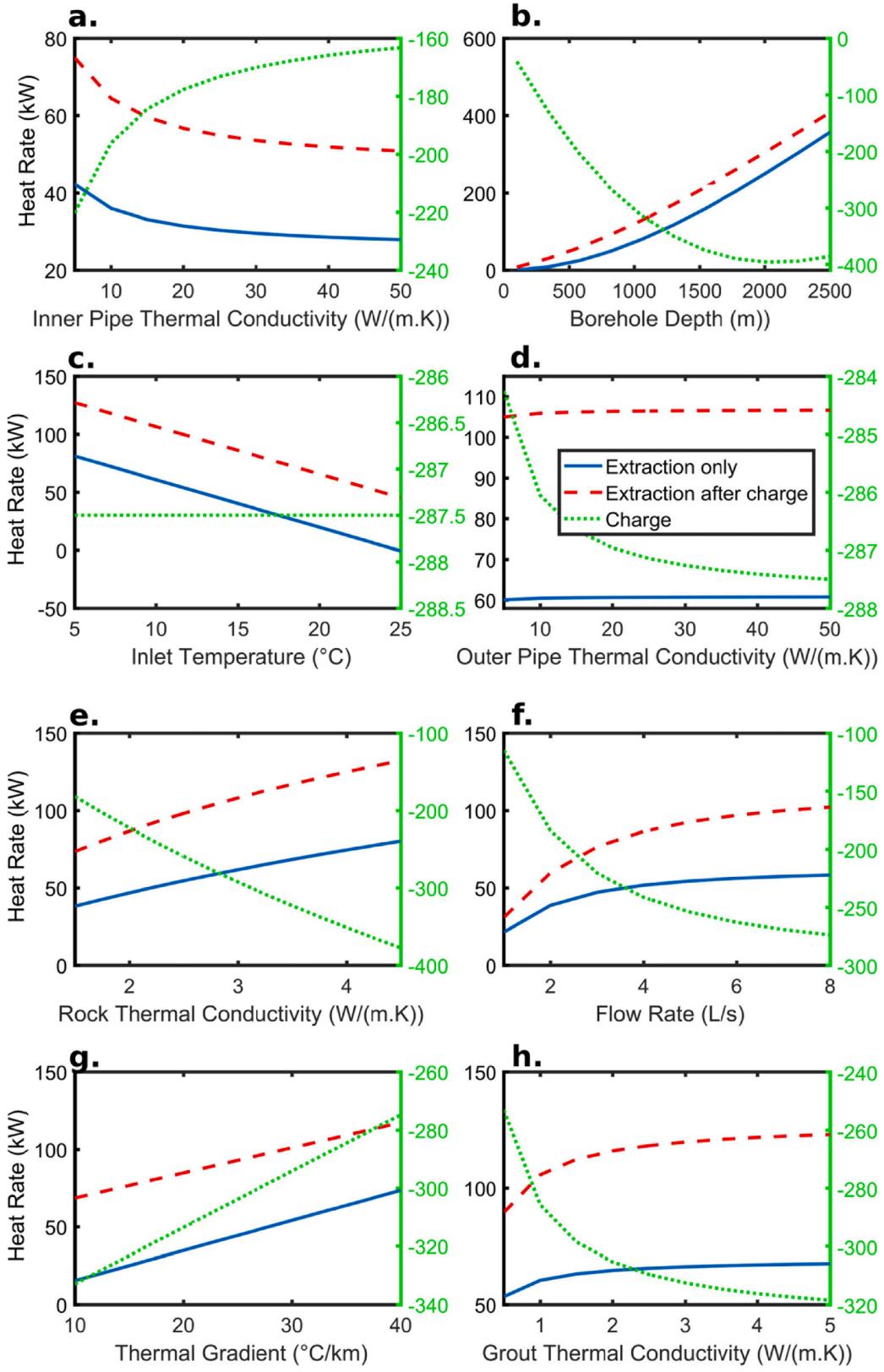

Fig. 8. Impact of parameterisation on average heat transfer rate (kW) including, (a) inner pipe thermal conductivity, (b) borehole depth, (c) inlet temperature during extraction, (d) outer pipe thermal conductivity, (e) rock thermal conductivity, (f) flow rate, (g) geothermal gradient and (h) grout thermal conductivity. Solid blue line indicates thermal power after extraction only for 6 months with a constant inlet temperature of 10 °C and red dashed line indicates thermal power after 6 months charge at 95 °C followed by 6 months extraction with a constant inlet temperature of 10 °C (left hand y axis). The dotted green axis corresponds to the heat rate during the period of charge and is negative to indicate that heat is stored in the subsurface (right hand y axis). (For interpretation of the references to colour in this figure legend, the reader is referred to the web version of this article.)

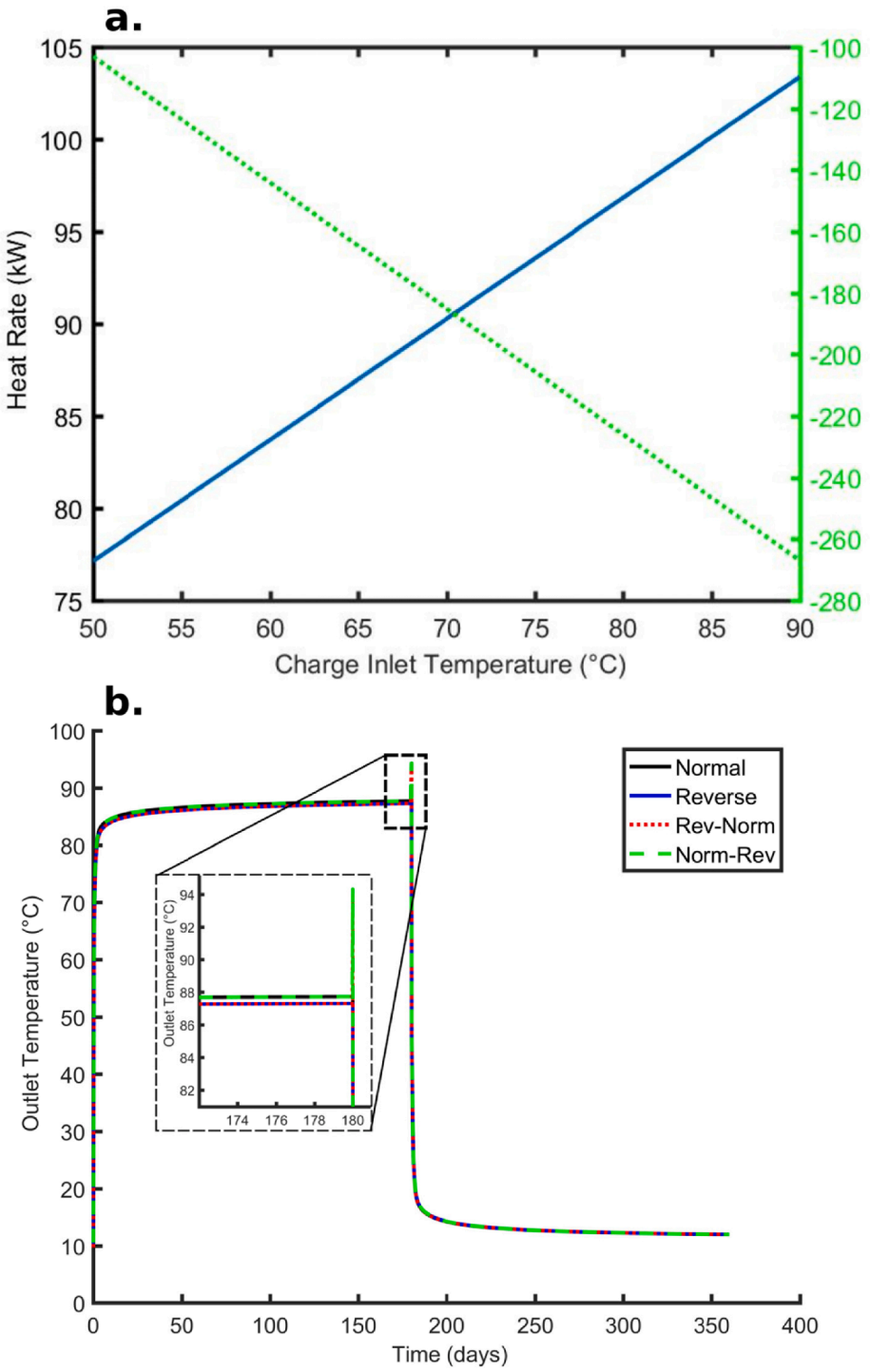

Fig. 9. (a) Impact of charge inlet on average heat rate (kW) during both energy storage period and extraction period. (b) Outlet temperatures for different flow direction. Note constant inlet temperature of 95 °C for the first 6 months and 10 °C for the second 6 months.

inlet temperature during extraction; where the Spearman coefficient value was greater than Pearson's (Fig. 12 and Table 3). This is likely to indicate the decrease in inlet temperature during extraction resulted in higher storage efficiency, but the amount of increase was not consistent.

Both methods provide similar rankings of parameter influence (Table 3) for each different aggregated evaluation parameter (Eqs. (6) and (7)). The most important parameters at determining 1) storage efficiency were geothermal gradient and extraction inlet temperature, 2) charge heat rate was charge inlet temperature and 3) extraction heat rate were extraction inlet temperature and flow rate. Conversely, the least important parameters at determining 1) storage efficiency were grout and inner pipe thermal conductivity, 2) charge heat rate was outer pipe thermal conductivity and 3) extraction heat rate were inner pipe and grout thermal conductivity. The least important parameters across all evaluation parameters appear to be associated to material thermal properties, whilst the most important parameters were associated to DBHE operation and also the geothermal gradient.

The results for the global sensitivity analysis produced similar conclusions to the local sensitivity analysis. A higher geothermal gradient led to higher storage efficiencies and heat rates. Extraction inlet

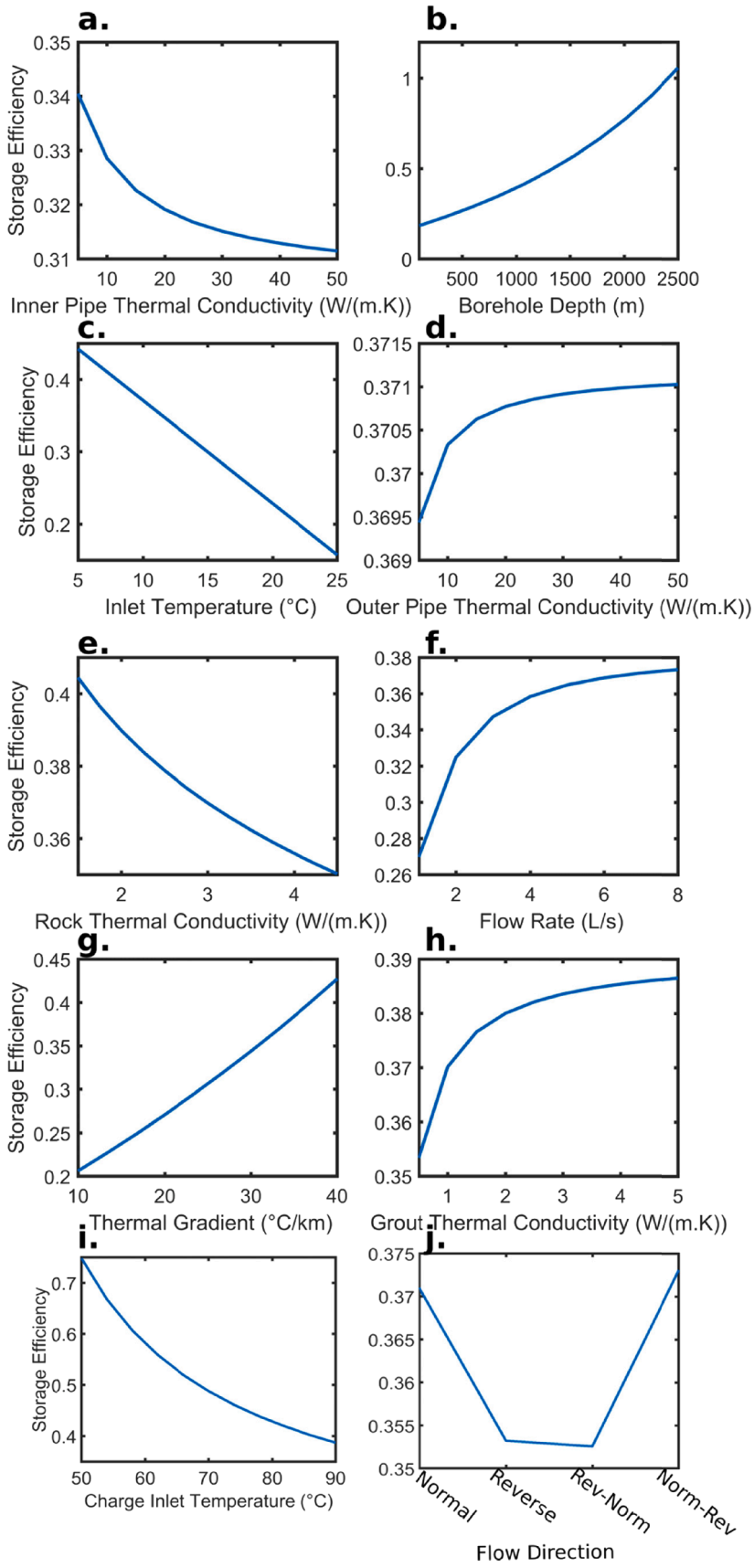

Fig. 10. Impact of parameterisation on storage efficiency including, (a) inner pipe thermal conductivity, (b) borehole depth, (c) inlet temperature during extraction, (d) outer pipe thermal conductivity, (e) rock thermal conductivity, (f) flow rate, (g) geothermal gradient, (h) grout thermal conductivity, (i) charge inlet temperature and (j) DBHE flow direction.

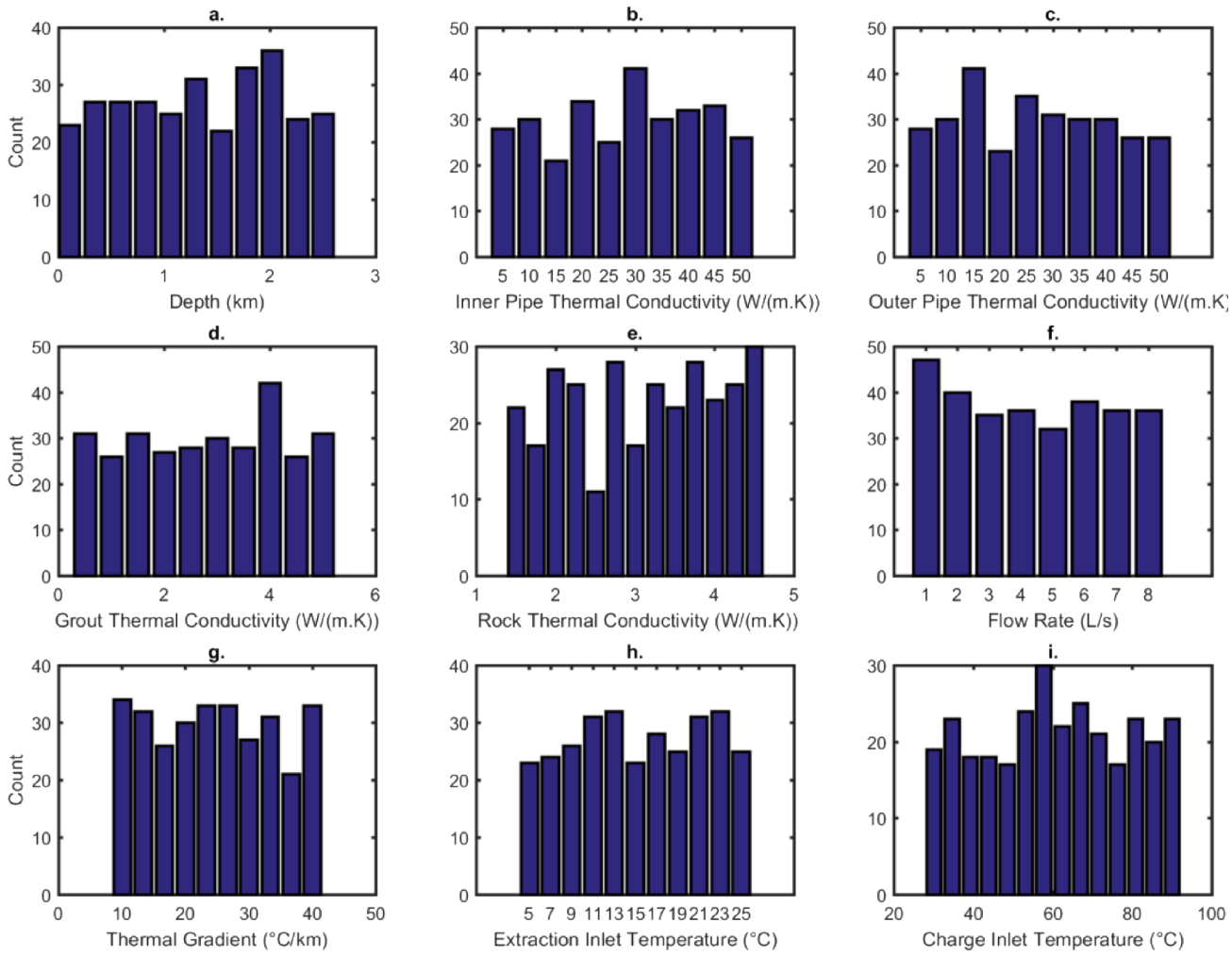

Fig. 11. Frequency density of parameters used for (a) borehole depth, (b) inner pipe thermal conductivity, (c) outer pipe thermal conductivity, (d) grout thermal conductivity, (e) rock thermal conductivity, (f) flow rate, (g) geothermal gradient, (h) inlet temperature during extraction, and (i) charge inlet temperature. Note the flow direction was distributed equally throughout with 75 simulations of each configuration.

temperatures did not impact charge, but the negative relationship observed in Fig. 12 indicates reduced heat rates were achieved under higher inlet temperatures during extraction. Increasing charge inlet temperatures led to more heat transfer, but this only had a minor impact on extraction, leading to poorer storage efficiency as less energy was recovered. Higher flow rates led to more heat transfer between the annular fluid and surrounding rock leading to better storage efficiencies.

3.3.2. *Flow direction*

The statistical methods used to rank the parameters importance were not applicable to different flow directions as numerical values cannot be assigned to determine the parametric input rank. To understand the significance of flow direction the dispersion of the data set was considered.

Fig. 13a highlights the distribution during charge, with negative skews in the data observed for each type of flow direction, whilst for extraction (Fig. 13b) positive skews were observed. The reverse flow direction appears to have better performance when transferring heat into the ground during charge (Fig. 13a); however, the reverse-normal flow configuration is poorest at transferring heat. This indicates different flow directions had little impact on results, similarly the extraction phase shows little influence on performance (Fig. 13b).

3.3.3. *Distribution of heat rate*

By using a probabilistic assessment and exploring the cumulative distribution function of the spread of data, confidence levels in the uncertainty of different parameters can be acquired. Utilising probability values corresponding to 10, 50 and 90 %, the distribution of heat rate during charge and extraction was determined.

The probability distribution for both charge and extraction average heat rates (Fig. 14 and Table 4) showed a relatively high range. The heat rate for charge exhibited a difference of 75 kW between each probability level, whilst for extraction it increased by 33 kW between the P90 and P50 estimates. It then increased by over double this (68 kW) for P50 to P10 estimates. Interestingly the lower 10 % probability level for average heat rate during extraction was negative and shows no heat was extracted, and in fact heat was lost. Upon closer inspection the values with negative heat rates appear to coincide with scenarios where the inlet extraction temperature was high and the average temperature in the system was low. Therefore, it highlights BTES systems are better deployed with the lowest inlet temperature possible during extraction and in areas of higher geothermal gradient. However, it is worth noting this may be less suitable for operational longevity and impact the sustainability due to higher thermal drawdown in the DBHE.

3.4. *Evaluation of storage efficiency metric*

Whilst the most common method of evaluating storage efficiency (Eq. (7)) is a useful metric it can lead to storage efficiencies exceeding 1 in deep BTES systems (Fig. 10b). Therefore, to test the potential of other

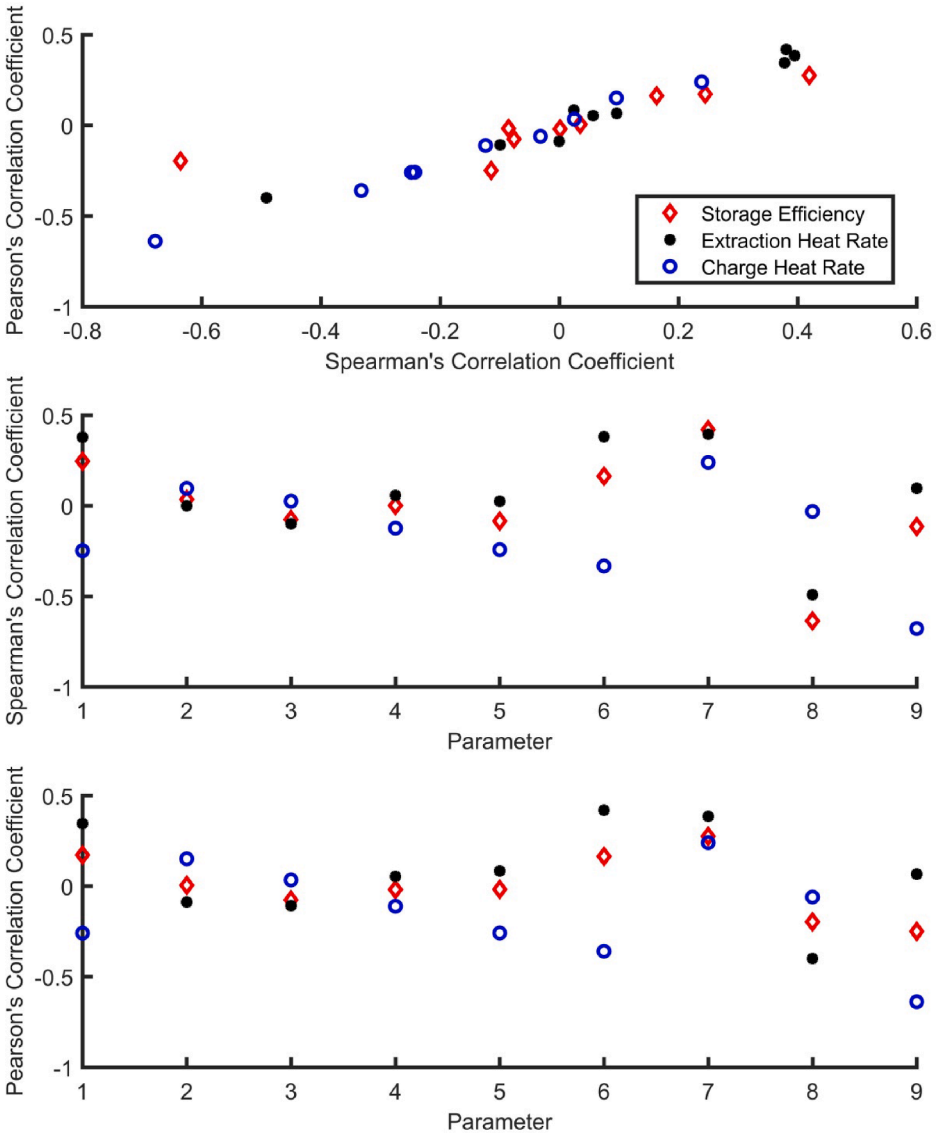

Fig. 12. Impact of parameterisation on storage efficiency, extraction heat rate (following charge) and charge heat rate. (a) Shows the relationships between Spearman's and Pearson's correlation. (b) Spearman's and (c) Pearson's correlation in relation to each parameter tested. Parameters are as follows: 1 = borehole depth, 2 = inner pipe thermal conductivity, 3 = outer pipe thermal conductivity, 4 = grout thermal conductivity, 5 = rock thermal conductivity, 6 = flow rate, 7 = geothermal gradient, 8 = inlet temperature during extraction, and 9 = charge inlet temperature.

Table 3
Rankings of parameter importance on storage efficiency, charge heat rate and extraction heat rate. The rankings are in descending order of importance (i.e., 1 is the most influential parameter and 9 is the least).

	Storage Efficiency Influence		Charge Heat Rate Influence		Extraction Heat Rate Influence	
Parameter	**Spearman's**	**Pearson's**	**Spearman's**	**Pearson's**	**Spearman's**	**Pearson's**
Borehole Depth	**3**	**4**	**3**	**3**	**4**	**4**
Inner Pipe Thermal Conductivity	**8**	**9**	**7**	**6**	**9**	**6**
Outer Pipe Thermal Conductivity	**7**	**6**	**9**	**9**	**5**	**5**
Grout Thermal Conductivity	**9**	**7**	**6**	**7**	**7**	**9**
Rock Thermal Conductivity	**6**	**8**	**4**	**4**	**8**	**7**
Flow Rate	**4**	**5**	**2**	**2**	**3**	**1**
Geothermal Gradient	**2**	**1**	**5**	**5**	**2**	**3**
Extraction Inlet Temperature	**1**	**3**	**8**	**8**	**1**	**2**
Charge Inlet Temperature	**5**	**2**	**1**	**1**	**6**	**8**

methods of evaluation (Eq. 7–9) a comparative analysis using the local parametric sensitivity data (section 3.2) was undertaken. The different metrics evaluate different aspects of BTES; Eq.7 evaluates the total energy entering and exiting the system during charge, Eq.8 evaluates the energy entering the system during charge and Eq.9 evaluates the difference in energy extracted after storage in comparison to extraction without charge.

Fig. 15 highlights the difference between these methods. As expected, Eq. (8) and (9) estimate reduced values for storage in comparison to Eq. (7). The new storage metric mirrors the commonly used shallow storage efficiency metric for thermal conductivity of different materials and flow rate. There is however, discrepancy between borehole depth, inlet temperature during extraction and geothermal gradient. When considering borehole depth, the increase in energy

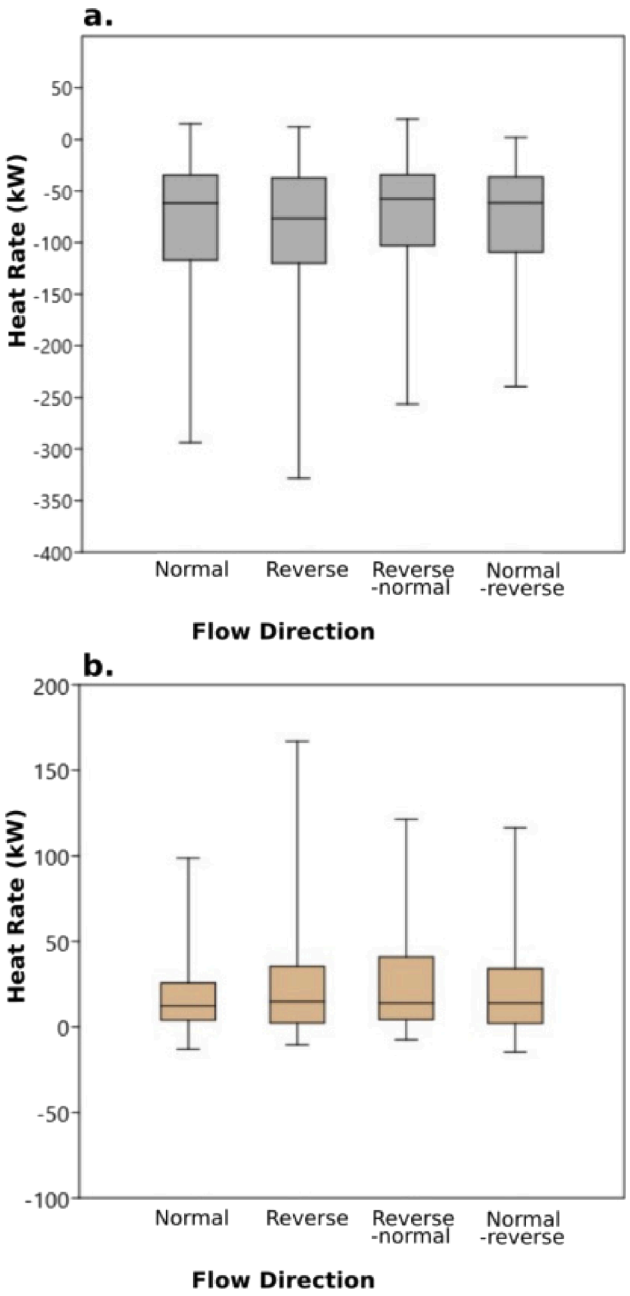

Fig. 13. Box and whisker plot showing the impact on flow direction for the average heat rates during (a) charge and (b) extraction. Note 75 different simulations for each configuration.

stored through charge was proportional to the increase in energy extracted, meaning the storage efficiency was relatively low and in fact had a slight decline with increased depths. The increase in inlet temperature (both charge and extraction) and geothermal gradient had a minimal impact on the overall storage using the new metric. When changing the inlet temperature during extraction, minimal impact was observed due to the average charge heat rate remaining constant throughout. When considering increased charge inlet temperatures, the increase in energy into the system was proportional to the energy extracted and therefore, did not significantly increase storage efficiency. For increased geothermal gradients the negative impact on charge was proportional to a minor overall increase in energy extraction.

Interestingly the metric used by Xie et al. [62] (Eq. (8)) had similar efficiencies in comparison to the new metric for grout and piping thermal conductivity, geothermal gradient, inlet temperature during charge

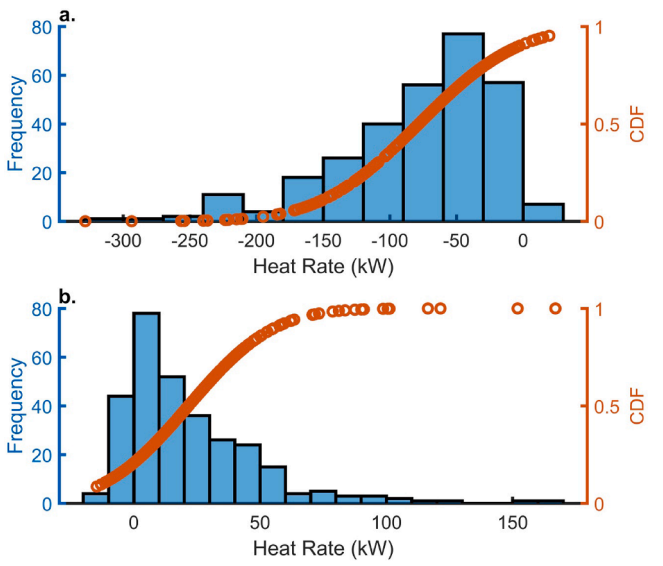

Fig. 14. Cumulative distribution function and distribution frequency of calculated average heat rates during (a) charge and (b) extraction.

Table 4
Probabilistic evaluation of Heat rate.

Heat Rate (kW)			
	P90	**P50**	**P10**
Charge	−153	−78	−3
Extraction	−11	22	90

and inlet temperature during extraction. This suggests that the impact of charge is most dominant on the overall impact to the system for these parameters. The discrepancy observed for varying flow rate, borehole depth and rock thermal conductivity was due to the fact this metric only evaluates the charge period. Therefore, it highlights that increased flow rates led to poorer efficiencies during charge. This appears to be an issue with the evaluation metric of Xie et al. [62] as it negates the impact of the mass flow rate (which cancels in the equation when constant). Borehole depth had a positive relationship to storage efficiency using this method, until the maximum heat rate was reached at ~ 2000 m. Similarly, rock thermal conductivity had a positive correlation with efficiency due to the increased amount of energy stored during charge.

When considering storage efficiency using the new metric, it was observed that the slight increase in energy stored during charge for the reverse flow direction (CXC) (Fig. 9b) does not actually significantly benefit the system. For the new metric, this led to lower storage efficiency than if a normal (CXA) flow direction was considered for operation during charge and extraction. Similarly, the other metrics showed little variation for the change of flow direction.

4. Discussion

4.1. Impact of charge on the Newcastle Science Central deep geothermal borehole heat exchanger performance

Results indicate that the Newcastle Science Central DBHE could supply a heat rate (after charge) of c. 69 kW to nearby buildings if repurposed to a depth of 920 m (measured under base case parameters at the end of the simulation – i.e., Table 1). The adjacent Urban Sciences Building demand has been modelled annually to range from 792 to 989 MWh [65]. Therefore, the DBHE could meet a significant proportion of the demand; whilst there is potential for summer months cooling demand to be coupled to the BTES system too.

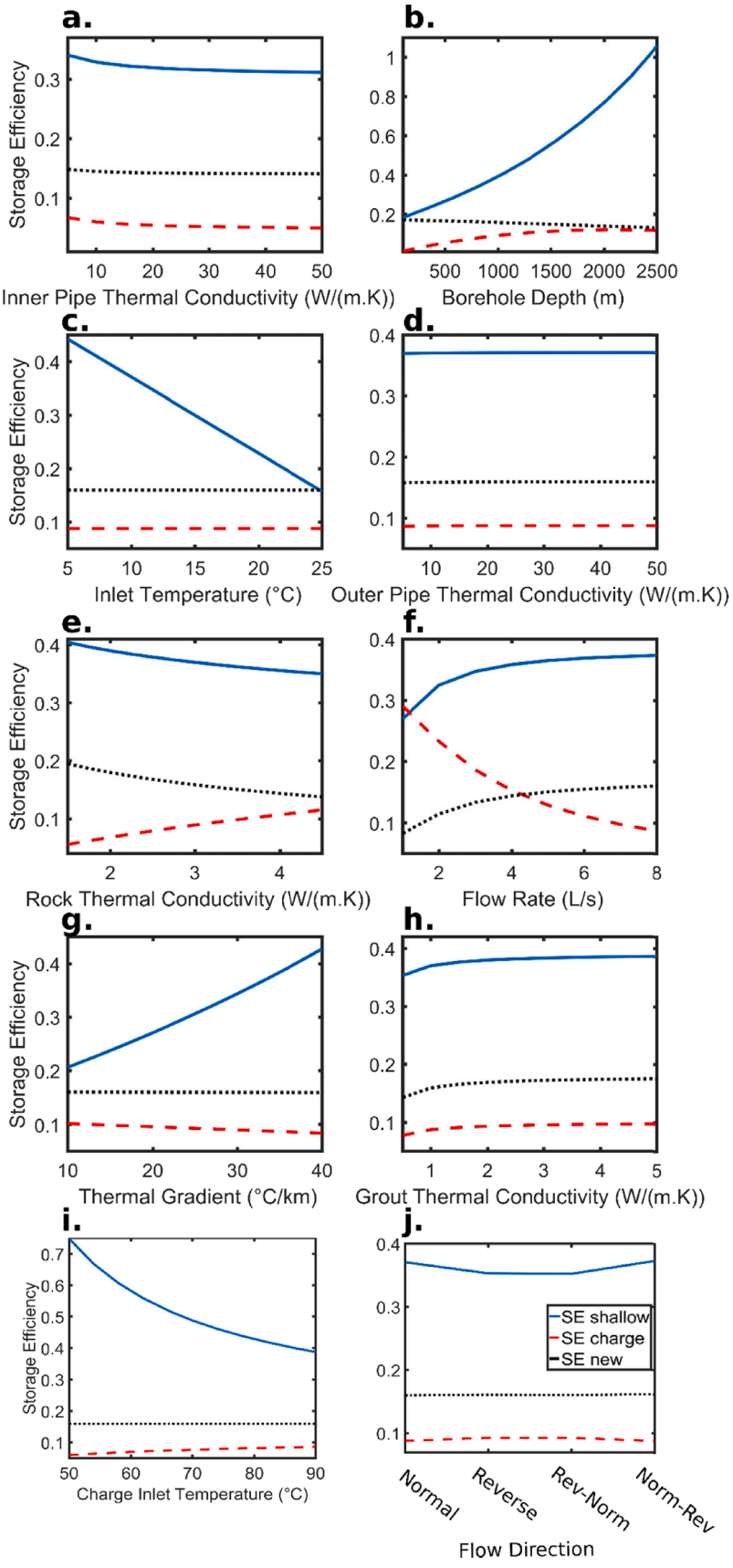

Fig. 15. Impact of parameterisation on different methods of calculating storage efficiency including, (a) inner pipe thermal conductivity, (b) borehole depth, (c) inlet temperature during extraction, (d) outer pipe thermal conductivity, (e) rock thermal conductivity, (f) flow rate, (g) geothermal gradient, (h) grout thermal conductivity, (i) charge inlet temperature and (g) flow direction. Solid blue line indicates method typically used in shallow systems, red dashed line indicates the method by Xie et al. [62] which only evaluates charge and the dotted black line is for the new metric used here. (For interpretation of the references to colour in this figure legend, the reader is referred to the web version of this article.)

In return for injection thermal rates of between −41.2 and −396.8 kW, energy storage appears to have a minor increase on the extraction rate, increasing it by 9.5–55.6 kW in comparison to the case without charge. This is when evaluating for a 6 month period of charge followed by 6 months of extraction. If considering the influence of BTES for a longer period it is likely that the heat rate during extraction could increase further as the charge period continues to build up the heat stores. Due to the low outlet temperatures, it is also likely a heat pump would be required to exploit the energy.

Geological parameters such as rock thermal conductivity and heat flow of the subsurface at Newcastle are likely to aid performance. Rock thermal conductivity in situ, ranges from 2 − 3 W/(m.K), and geothermal gradients are high in the area due to the proximity of the North Pennine Batholith [64,33]. The geothermal gradient for the full length of the NSCDGB is c. 37 °C/km, whilst for the upper 920 m is closer to c. 33.4 °C/km, which is line with the Longhorsley Borehole [28,64]. Therefore, at greater depths performance is likely to improve due to the higher temperatures from the geothermal gradient. To optimise performance, further studies should focus on operational parameters shown to have the most significant impact on performance. These include inlet temperature and flow rate.

Although it was not ranked as the most important factor during the global sensitivity analysis, borehole depth was proven to be important in local sensitivity simulations. Borehole depth allows the DBHE to operate with higher heat rates during charge and extraction. Therefore, if it is feasible or economically possible to repurpose the DBHE to a depth of c. 1600 m, it would benefit the overall performance and maximise the heat transfer area.

4.2. Comparison of global and local sensitivity analysis

Although the local and global sensitivity analysis identified key parameters using qualitative and quantitative methods respectively, both recognised similar key parameters. During the local sensitivity analysis, the parameters that had the most significant range of heat rates were borehole depth, rock thermal conductivity, geothermal gradient, flow rate and inlet temperatures. This was also reflected when evaluating storage efficiency; however, rock thermal conductivity only had a minor range between the minimum and maximum parametric inputs.

For the global simulations, the top ranked parameters based on average heat rate and storage efficiency were geothermal gradient, flow rate and inlet temperature. Borehole depth was deemed to be less important, but did consistently score in the top 4 most influential parameters. Based on the analysis of this study it appears that local and global sensitivity analysis draw similar conclusions.

4.3. Significance of relationships identified using Spearman's Rank and Pearson's Correlation Coefficient

It is important to understand the correlation and significance of the statistical methods used. Using Spearman's Rank Correlation Coefficient the parameters ranked at: a) 1–4 for the extraction heat rate had observed p-values of less than 1.2e-11, b) 1–6 for the charge heat rate had observed p-values of less than 0.032 and c) 1–5 for the storage efficiency had observed p-values of less than 0.048. As the aforementioned parameters were less than 0.05, it can be concluded that results are likely to be reliable. All other variables for Spearman's Rank correlation have p-values in excess of 0.05, indicating the less influential parameters were not statistically significant. Similarly, when considering results for Pearson's Correlation Coefficient, it can be concluded that ranked parameters a) 1–4 for heat extraction, b) 1–6 for charge and c) 1–5 for storage efficiency were significant findings.

4.4. Evaluation of performance indicators

The typical method of evaluating energy storage in BTES systems (Eq. (7)) provides a useful indicator for the performance of a DBHE. However, during the global and local sensitivity analysis, some parameters highlighted storage efficiency could exceed the value of 1, meaning more heat was extracted than stored. Also, the method of evaluating storage does not consider whether storage is efficient as it is based on the ratio of difference in total thermal power between the inlet and outlet during charge and extraction periods. Therefore, factors that influence charge or extraction may result in high efficiencies, which may be in contrast to the true nature of storage which may be poor. This indicates the method may not be suitable to evaluate the efficiency of deep BTES systems.

A metric provided by Xie et al. [62] to evaluate deep BTES (Eq. (8)) was also considered. This provided a useful method to consider the efficiency during charge alone, but does not consider the efficiency of the whole system (i.e., during extraction too) and this is reflected when comparing this to the most commonly used metric for storage efficiency (Eq. (7)). Furthermore, when considering altering mass flow rates it implies that increasing flow rate reduces the efficiency, when in contrast the two alternative metrics and the heat rate during charge suggest the opposite. This is because the mass flow rate is not considered when constant.

In this study, we have suggested a potential alternate method for deep BTES systems which evaluates the increased heat extracted due to charge in comparison to without charge (i.e., extraction only) (Eq. (9)). It therefore, directly considers the impact of storage, rather than the total efficiency of the system (such as that in Eq. (7)). It could prove a useful performance indicator for storage in a system in future studies. However, there are practical considerations for 'real' studies such as the operational considerations where these systems may require a pre-charge period and/or may not have the data to evaluate performance without charge. In these cases, it may be best to use Eq. (7), but to consider it as an indicator of system efficiency, rather than storage efficiency.

5. Conclusions

This paper presents a modelling study that highlights the potential for DBHEs to be operated as dual purpose for thermal energy storage and heat extraction. Previously, few studies have investigated deep BTES from a single DBHE or the repurposing of ex-geothermal exploration wells. The model used was developed on MATLAB by Brown et al. [15] and has been verified further by comparing to the established OpenGeoSys software. A discrepancy in outlet temperature of less than 0.3 % indicates strong performance in comparison. Subsequently, a local and global sensitivity analysis was performed to understand the impacts of a range of parameters on the operation of a DBHE for BTES. Pearson's and Spearman's Correlation Coefficients were used to determine the influence of different parameters on storage efficiency. Finally, different storage metrics were investigated as previous metrics are more suited to shallow systems. The key conclusions for the study were:

- Under the initial base case scenario the minimum heat rate during charge was −250 kW and 69 kW during extraction (measured at the end of each period). Thermal propagation was minor and less than 19 m from the DBHE for the duration of the simulations.
- Heat rate during extraction was increased by 9.5–55.6 kW if it followed a 6 month period of charge. The charge period in this study represents the typical heating period in the UK. In other locations it is likely to differ. Therefore, varying the temporal duration for charge or extraction is likely to influence results and could be focused on in future work.
- Local sensitivity analysis highlighted the most important parameters to be borehole depth, geothermal gradient, flow rate, inlet temperature during charge and extraction. Using the metric typically used in past literature for storage efficiency (Eq. (7)), the maximum range in efficiency was observed for charge inlet temperature, where for

the lowest charge inlet temperature efficiency increased by 0.36 in contrast to the maximum charge temperature (Fig. 10i). Global sensitivity analysis draws similar conclusions to the local sensitivity analysis. These parameters should be focused on in planning and design of deep BTES systems universally.

- Operational parameters were more influential on deep BTES systems than thermal conductivities of materials. This was highlighted by analysis using Spearman's and Pearson's Correlation Coefficients (Table 3). This conclusion was also supported by local sensitivity analysis.
- Flow direction (i.e., normal v reverse flow direction or CXA v CXC) had little impact on model results. The median values (Fig. 13) were all within 19 kW for global simulations, whilst for the local sensitivity analysis the end temperature was within 0.03 °C.
- Although the amount of heat energy recovered from that injected was modest, results give scope for further investigation into the repurposing of abandoned or nearing end of life oil and gas wells across the UK for BTES, particularly if there is nearby surplus heat. Alternatively, DBHEs can be utilised for de-risking geothermal wells if the reservoir conditions in hydrothermal conditions are not suitable for open-loop development.
- An alternative metric (Eq. (9)) has been identified to evaluate storage efficiency of deep and also shallow BTES systems. This shows the increase in system performance after charge, in contrast to operation of a DBHE without charge. As a result, the storage efficiency calculated is far lower than the conventional metric used for evaluating shallow systems.

Future work should aim to investigate parameter impact under long term simulations for a lifetime of a BTES system, including a period of pre-charge, as this could lead to an increase in storage efficiency. It should also consider coupling to the surface demand (e.g., [38,39]).

Declaration of Competing Interest

The authors declare that they have no known competing financial interests or personal relationships that could have appeared to influence the work reported in this paper.

Data availability

Data will be made available on request.

Acknowledgments

We would like to show appreciation to the UKRI EPSRC (grant reference numbers EPSRC EP/T022825/1 and EPSRC EP/T023112/1) for funding this research. The funding sources are for the NetZero GeoRDIE (Net Zero Geothermal Research for District Infrastructure Engineering) and INTEGRATE (Integrating seasoNal Thermal storagE with multiple enerGy souRces to decArobonise Thermal Energy) projects, respectively. For the purpose of open access, the author has applied a Creative Commons Attribution (CC BY) licence to any Author Accepted Manuscript version arising from this submission. The authors would also like to thank three anonymous reviewers and the editor for their useful comments which have helped to improve the paper.

References

[1] R. Al-Khoury, Computational modeling of shallow geothermal systems, CRC Press, 2011.
[2] R. Al-Khoury, P.G. Bonnier, B.J. Brinkgreve, Efficient finite element formulation for geothermal heating systems. Part I: steady state, Int. J. Numerical Methods Eng. 63 (2005) 988–1013. 10.1002/nme.1313.
[3] R. Al-Khoury, P.G. Bonnier, Efficient finite element formulation for geothermal heating systems. Part II: transient, Int. J. Numerical Methods Eng. 67 (2006) 725–745, https://doi.org/10.1002/nme.1662.
[4] R. Al-Khoury, T. Kolbel, R. Schramedei, Efficient numerical modeling of borehole heat exchangers, Comput. Geosci. 36 (10) (2010) 1301–1315, https://doi.org/10.1016/j.cageo.2009.12.010.
[5] C. Alimonti, D. Berardi, D. Bocchetti, E. Soldo, Coupling of energy conversion systems and wellbore heat exchanger in a depleted oil well, Geothermal Energy 4 (1) (2016) 1–17.
[6] O. Andersson, N. Håkansson, L. Rydell, Heat pumps rescued Xylem's heat storage facility in Emmaboda, Sweden. REHVA Journal 58 (4) (2021) 23–27.
[7] O. Andersson, L. Rydell, N. Håkansson, Heat pump system improved high-temperature borehole thermal energy storage efficiency, Heat Pumping Technologies 40 (2) (2021) 21–23.
[8] D. Banks, Thermal properties of well construction materials - Newcastle Science Central borehole. Internal University of Glasgow report for NetZero GeoRDIE project: unpublished, 2021.
[9] F. Behbehani, J.S. McCartney, Energy Pile Groups for Thermal Energy Storage in Unsaturated Soils, Appl. Therm. Eng. (2022), 119028.
[10] B. Bezyan, S. Porkhial, A.A. Mehrizi, 3-D simulation of heat transfer rate in geothermal pile-foundation heat exchangers with spiral pipe configuration, Appl. Therm. Eng. 87 (2015) 655–668.
[11] A.A. Mehrizi, S. Porkhial, B. Bezyan, H. Lotfizadeh, Energy pile foundation simulation for different configurations of ground source heat exchanger, Int. Commun. Heat Mass Transfer 70 (2016) 105–114.
[12] M.H.P. Bott, G.A.L. Johnson, J. Mansfield, J. Wheilden, Terrestrial heat flow in north-east England, Geophys. J. Roy. Astronomical Soc. 27 (1972) 277–288.
[13] BRE, Report 4: Main heating systems. Prepared by BRE on behalf of the Department of Energy and Climate Change BRE report number 286733a, 2013, https://assets.publishing.service.gov.uk/government/uploads/system/uploads/attachment_data/file/274772/4_Main_heating_systems.pdf (accessed on 30/2/2022).
[14] C.S. Brown, Modelling, characterisation and optimisation of deep geothermal energy in the Cheshire basin, Doctoral dissertation, University of Birmingham, 2020.
[15] C.S. Brown, N.J. Cassidy, S.S. Egan, D. Griffiths, Numerical modelling of deep coaxial borehole heat exchangers in the Cheshire Basin, UK, Comput. Geosci. 152 (2021), 104752.
[16] C.S. Brown, N.J. Cassidy, S.S. Egan, D. Griffiths, A sensitivity analysis of a single extraction well from deep geothermal aquifers in the Cheshire Basin, UK, Quarterly J. Eng. Geol. Hydrogeol. (2022), https://doi.org/10.1144/qjegh2021-131.
[17] C.S. Brown, N.J. Cassidy, S.S. Egan, D. Griffiths, Thermal and Economic Analysis of Heat Exchangers as Part of a Geothermal District Heating Scheme in the Cheshire Basin, UK. Energies 15 (6) (2022) 1983.
[18] C.S. Brown, Regional geothermal resource assessment of hot dry rocks in Northern England using 3D geological and thermal models, Geothermics 105 (2022), 102503.
[19] N. Catolico, S. Ge, J.S. McCartney, Numerical modeling of a soil-borehole thermal energy storage system, Vadose Zone Journal 15 (1) (2016).
[20] C. Chen, H. Shao, D. Naumov, Y. Kong, K. Tu, O. Kolditz, Numerical investigation on the performance, sustainability, and efficiency of the deep borehole heat exchanger system for building heating, Geothermal Energy 7 (1) (2019) 1–26.
[21] L. Dijkshoorn, S. Speer, R. Pechnig, Measurements and design calculations for a deep coaxial borehole heat exchanger in Aachen, Germany, Int. J. Geophys. 2013 (2013).
[22] H.J. Diersch, D. Bauer, W. Heidemann, W. Rühaak, P. Schätzl, Finite element modeling of borehole heat exchanger systems: Part 1. Fundamentals, Comput. Geosci. 37 (8) (2011) 1122–1135.
[23] H.J. Diersch, D. Bauer, W. Heidemann, W. Rühaak, P. Schätzl, Finite element modeling of borehole heat exchanger systems: Part 2. Numerical simulation, Comput. Geosci. 37 (8) (2011) 1136–1147.
[24] H.R. Doran, T. Renaud, G. Falcone, L. Pan, P.G. Verdin, Modelling an unconventional closed-loop deep borehole heat exchanger (DBHE): sensitivity analysis on the Newberry volcanic setting, Geothermal Energy 9 (1) (2021) 1–24.
[25] P.C. England, E.R. Oxburgh, S.W. Richardson, Heat refraction and heat production in and around granite plutons in north–east England, Geophys. J. Int. 62 (1980) 439–455.
[26] G. Falcone, X. Liu, R.R. Okech, F. Seyidov, C. Teodoriu, Assessment of deep geothermal energy exploitation methods: The need for novel single-well solutions, Energy 160 (2018) 54–63, https://doi.org/10.1016/j.energy.2018.06.144.
[27] P. Fleuchaus, B. Godschalk, I. Stober, P. Blum, Worldwide application of aquifer thermal energy storage–A review, Renewable Sustainable Energy Rev. 94 (2018) 861–876.
[28] J.S. Gebski, J. Wheildon, A. Thomas-Betts, Investigations of the UK heat flow field (1984-1987). Report WJ/GE/87/6, British Geological Survey, Nottingham, 60 pp, 1987.
[29] GOW, 2020. Grants on the web. EPSRC EP/T022825/1. Accessed on 11/4/2022: https://gow.epsrc.ukri.org/NGBOViewGrant.aspx?GrantRef=EP/T022825/1.
[30] A.J. Kallesøe, T. Vangkilde-Pedersen, L. Guglielmetti, HEATSTORE Underground Thermal Energy Storage (UTES)–state-of-the-art, example cases and lessons learned, 2019.
[31] Y. He, X. Bu, A novel enhanced deep borehole heat exchanger for building heating, Appl. Therm. Eng. 178 (2020), 115643.
[32] P. Hein, O. Kolditz, U.-J. Görke, A. Bucher, H. Shao, A numerical study on the sustainability and efficiency of borehole heat exchanger coupled ground source heat pump systems, Appl. Therm. Eng. 100 (2016) 421–433, https://doi.org/10.1016/j.applthermaleng.2016.02.039.

[33] L. Howell, C.S. Brown, S.S. Egan, Deep geothermal energy in northern England: Insights from 3D finite difference temperature modelling, Comput. Geosci. 147 (2021), 104661.
[34] M. Lanahan, P.C. Tabares-Velasco, Seasonal thermal-energy storage: A critical review on BTES systems, modeling, and system design for higher system efficiency, Energies 10 (6) (2017) 743.
[35] M. Le Lous, F. Larroque, A. Dupuy, A. Moignard, P.C. Damy, Performance of an open-loop well-doublet scheme located in a deep aquitard–aquifer system: Insights from a synthetic coupled heat and flow model, Geothermics 74 (2018) 74–91.
[36] B. Lesniak, Ł. Słupik, G. Jakubina, The determination of the specific heat capacity of coal based on literature data, Chemik 67 (2013) 560–571.
[37] Y. Luo, G. Xu, S. Zhang, N. Cheng, Z. Tian, J. Yu, Heat extraction and recover of deep borehole heat exchanger: Negotiating with intermittent operation mode under complex geological conditions, Energy (2021), 122510.
[38] A. Lyden, R. Pepper, P.G. Tuohy, A modelling tool selection process for planning of community scale energy systems including storage and demand side management, Sustainable Cities Soc. 39 (2018) 674–688.
[39] A. Lyden, C.S. Brown, I. Kolo, G. Falcone, D. Friedrich, Seasonal thermal energy storage in smart energy systems: District-level applications and modelling approaches, Renewable Sustainable Energy Rev. 167 (2022), 112760.
[40] J. Liu, F. Wang, W. Cai, Z. Wang, Q. Wei, J. Deng, Numerical study on the effects of design parameters on the heat transfer performance of coaxial deep borehole heat exchanger, Int. J. Energy Res. (2019) 1–16, https://doi.org/10.1002/er.435716LIUETAL.
[41] M. Nabi, R. Al-Khoury, An efficient finite volume model for shallow geothermal systems. Part I: Model formulation, Comput. Geosci. 49 (2012) 290–296, https://doi.org/10.1016/j.cageo.2012.03.019 261.
[42] M. Nabi, R. Al-Khoury, An efficient finite volume model for shallow geothermal systems—Part II: Verification, validation and grid convergence, Comput. Geosci. 49 (2012) 297–307, https://doi.org/10.1016/j.cageo.2012.03.023.
[43] D.A. Nield, A. Bejan, Convection in a Porous Media, 408, Springer-Verlag, New York, 1992.
[44] OFGEM, Non-Domestic Renewable Heat Incentive (RHI); Office of Gas and Electricity Markets: London, UK, 2020. Available online: https://www.ofgem.gov.uk/environmental-programmes/non-domestic-rhi (accessed on 25 June 2020).
[45] P. Pasquier, A. Zarrella, D. Marcotte, A multi-objective optimization strategy to reduce correlation and uncertainty for thermal response test analysis, Geothermics 79 (2019) 176–187.
[46] I. Perser, I.A. Frigaard, A Comprehensive Study on Intermittent Operation of Horizontal Deep Borehole Heat Exchangers, Energies 15 (1) (2022) 307.
[47] T. Renaud, P.G. Verdin, G. Falcone, Conjugated numerical approach for modelling DBHE in high geothermal gradient environments, Energies 13 (22) (2020) 6107.
[48] T. Renaud, L. Pan, H. Doran, G. Falcone, P.G. Verdin, Numerical analysis of enhanced conductive deep borehole heat exchangers, Sustainability 13 (12) (2021) 6918.
[49] A. Rosato, A. Ciervo, G. Ciampi, M. Scorpio, S. Sibilio, Impact of seasonal thermal energy storage design on the dynamic performance of a solar heating system serving a small-scale Italian district composed of residential and school buildings, J. Energy Storage 25 (2019), 100889.
[50] H. Shao, P. Hein, A. Sachse, O. Kolditz, Geoenergy modeling II: shallow geothermal systems, Springer International Publishing, 2016.
[51] H. Skarphagen, D. Banks, B.S. Frengstad, H. Gether, Design considerations for borehole thermal energy storage (BTES): A review with emphasis on convective heat transfer, Geofluids 2019 (2019).
[52] S.M. Watson, G. Falcone, R. Westaway, Repurposing hydrocarbon wells for geothermal use in the UK: The onshore fields with the greatest potential, Energies 13 (14) (2020) 3541.
[53] S.M. Watson, G. Falcone, R. Westaway, Repurposing Hydrocarbon Wells for Geothermal Use in the UK: a Preliminary Resource Assessment. In: World Geothermal Conference 2020+1, Reykjavik, Iceland, 24-27 October 2021, 2021.
[54] B. Welsch, W. Rühaak, D.O. Schulte, K. Bär, S. Homuth, I. Sass, April. A comparative study of medium deep borehole thermal energy storage systems using numerical modelling. In Proceedings world geothermal congress, 2015.
[55] B. Welsch, W. Ruehaak, D.O. Schulte, K. Baer, I. Sass, Characteristics of medium deep borehole thermal energy storage, Int. J. Energy Res. 40 (13) (2016) 1855–1868.
[56] R. Westaway, P.L. Younger, Unravelling the relative contributions of climate change and ground disturbance to subsurface temperature perturbations: case studies from Tyneside, UK, Geothermics 64 (2016) 490–515.
[57] R. Westaway, Deep geothermal single well heat production: critical appraisal under UK conditions, Quart. J. Eng. Geol. Hydrogeol. 51 (4) (2018) 424–449.
[58] R. Westaway, Rock thermal properties for Newcastle Helix site. Internal University of Glasgow report for NetZero GeoRDIE project: unpublished, 2020.
[59] J. Wołoszyn, Global sensitivity analysis of borehole thermal energy storage efficiency for seventeen material, design and operating parameters, Renewable Energy 157 (2020) 545–559.
[60] J. Wołoszyn, Global sensitivity analysis of borehole thermal energy storage efficiency on the heat exchanger arrangement, Energy Convers. Manage. 166 (2018) 106–119.
[61] Z.H. Xia, G.S. Jia, Z.D. Ma, J.W. Wang, Y.P. Zhang, L.W. Jin, Analysis of economy, thermal efficiency and environmental impact of geothermal heating system based on life cycle assessments, Applied Energy 303 (2021), 117671.
[62] K. Xie, Y.L. Nian, W.L. Cheng, Analysis and optimization of underground thermal energy storage using depleted oil wells, Energy 163 (2018) 1006–1016.
[63] L. Xu, J.I. Torrens, F. Guo, X. Yang, J.L. Hensen, Application of large underground seasonal thermal energy storage in district heating system: A model-based energy performance assessment of a pilot system in Chifeng, China, Appl. Therm. Eng. 137 (2018) 319–328.
[64] P.L. Younger, D.A. Manning, D. Millward, J.P. Busby, C.R. Jones, J.G. Gluyas, Geothermal exploration in the Fell Sandstone Formation (Mississippian) beneath the city centre of Newcastle upon Tyne, UK: the Newcastle Science Central deep geothermal borehole, Quart. J. Eng. Geol. Hydrogeol. 49 (4) (2016) 350–363.
[65] M. Zirak, M. Royapoor, T. Gilbert, Cross-platform energy modeling for scalable urban energy simulation: A case-study. In International Conference on Innovative Applied Energy (IAPE 2019). Newcastle University, 2019.
[66] G.S. Kimbell, R.M. Carruthers, A.S.D. Walker, J.P. Williamson, Regional geophysics of southern Scotland and northern England. Version 1.0 on CD-ROM. British Geological Survey, Keyworth, 2006. Available from: .